JCI The Journal of Clinical Investigation

# Itaconate suppresses atherosclerosis by activating a Nrf2-dependent anti-inflammatory response in macrophages in mice

Jianrui Song, … , Morgan Salmon, Daniel R. Goldstein

*J Clin Invest.* 2023. https://doi.org/10.1172/JCI173034.

Research In-Press Preview Cardiology Inflammation

## Graphical abstract

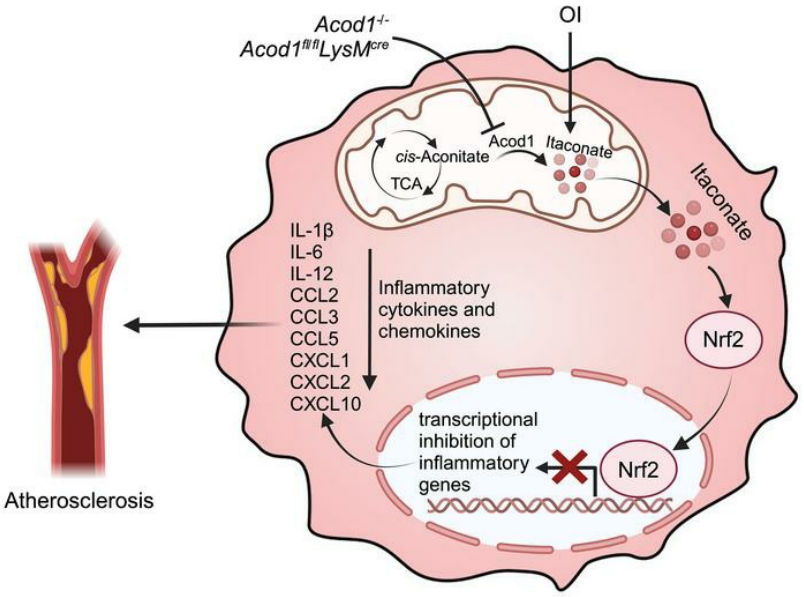

# Itaconate suppresses atherosclerosis by activating a Nrf2-dependent anti-inflammatory response in macrophages in mice

Jianrui Song[1,†], Yanling Zhang[2,†], Ryan A. Frieler[3], Anthony Andren[3], Sherri Wood[1], Daniel J. Tyrrell[1,4], Peter Sajjakulnukit[3,5], Jane C. Deng[6,7,8], Costas A. Lyssiotis[3,8,9], Richard M. Mortensen[3,10,11], Morgan Salmon[12] and Daniel R. Goldstein[1,6,13,14]

1. Department of Internal Medicine, Division of Cardiovascular Medicine, University of Michigan, Ann Arbor, MI 48109, USA
2. Department of Biochemistry and Molecular Biology, Soochow University Medical College, Suzhou, Jiangsu 215123, China
3. Department of Molecular and Integrative Physiology, University of Michigan, Ann Arbor, MI 48109, USA
4. Department of Pathology, Heersink School of Medicine, University of Alabama at Birmingham, AL 35205, USA
5. University of Michigan Rogel Cancer Center, University of Michigan, Ann Arbor, MI 48109, USA
6. Graduate Program in Immunology, University of Michigan, Ann Arbor, MI USA
7. Department of Internal Medicine, Division of Pulmonary and Critical Care Medicine, University of Michigan, Ann Arbor, MI 48109, USA
8. Veterans Affairs Ann Arbor Healthcare System, Ann Arbor, MI 48105, USA
9. Department of Internal Medicine, Division of Gastroenterology, University of Michigan Medical School, Ann Arbor, MI 48109, USA
10. Department of Pharmacology, University of Michigan, Ann Arbor, MI 48109, USA.
11. Department of Internal Medicine, Division of Metabolism, Endocrinology, and Diabetes, University of Michigan, Ann Arbor, MI 48109, USA.
12. Department of Cardiac Surgery, University of Michigan, Ann Arbor, MI 48109, USA
13. Department of Microbiology and Immunology, University of Michigan, MI 48109, USA
14. Address for correspondence: Daniel R. Goldstein, University of Michigan, Ann Arbor, MI 48109, USA. Phone: 734-936-1193. Email: drgoldst@umich.edu

[†]These authors share the first authorship.

**Abbreviated title:**
Macrophage itaconate suppresses atherosclerosis.

**Key words:**
Itaconate, Macrophage, Inflammation, Nrf2, Atherosclerosis

**Abstract**

Itaconate has emerged as a critical immunoregulatory metabolite. Here, we examined the therapeutic potential of itaconate in atherosclerosis. We found that both itaconate and the enzyme that synthesizes it, aconitate decarboxylase 1 (Acod1, also known as "immune-responsive gene 1"/IRG1) are upregulated during atherogenesis in mice. Deletion of *Acod1* in myeloid cells exacerbated inflammation and atherosclerosis in vivo and resulted in an elevated frequency of a specific subset of M1-polarized proinflammatory macrophages in the atherosclerotic aorta. Importantly, Acod1 levels were inversely correlated with clinical occlusion in atherosclerotic human aorta specimens. Treating mice with the itaconate derivative 4-ocytyl itaconate attenuated inflammation and atherosclerosis induced by high cholesterol. Mechanistically, we found that the antioxidant transcription factor, Nuclear factor erythroid-2 Related Factor 2 (Nrf2) was required for itaconate to suppress macrophage activation induced by oxidized lipids in vitro and to decrease atherosclerotic lesion areas in vivo. Overall, our work shows that itaconate suppresses atherogenesis by inducing Nrf2-dependent inhibition of proinflammatory responses in macrophages. Activation of the itaconate pathway may represent an important approach to treat atherosclerosis.

## Introduction

Itaconate has emerged as a compelling immunomodulatory metabolite produced in the tricarboxylic acid (TCA) cycle (1, 2). The enzyme *cis*-aconitate decarboxylase 1 (Acod1, also named Irg1) is responsible for itaconate synthesis and is highly expressed in macrophages. Studies of pre-clinical mouse models suggest that Acod1 and itaconate attenuate various non-infectious inflammatory conditions that involve macrophages, such as psoriasis (3), ischemia reperfusion injury of both brain and heart (4, 5), lung fibrosis (6) and abdominal aortic aneurysms (7). More recently, it was reported that Acod1 contributes to the immunosuppressive function of tumor-associated macrophages and diminishes the efficacy of cancer immunotherapy (8). Additionally, Acod1 was shown to suppress cardiac inflammation and fibrosis after acute myocardial infarction and chemotherapeutic drug exposure (9).

Itaconate is typically produced by macrophages to inhibit proinflammatory responses at several levels. These include inhibition of glycolysis, inhibition of succinate dehydrogenase and thus ROS generation by mitochondria, and suppression of the NLRP3 inflammasome (10, 11). Itaconate also upregulates anti-oxidant pathways, for instance, by positively regulating the Nuclear factor erythroid-2 Related Factor 2 (Nrf2) transcription factor (12, 13) and Activating Transcription Factor 3 (ATF3) (14). Ultimately, itaconate suppresses macrophages' ability to produce several proinflammatory cytokines, whereas *Acod1*-deficient macrophages exhibit an increased production of such cytokines (4). Hence, previous studies suggest that itaconate acts as a brake to restrain macrophage inflammatory responses.

Macrophages are key driver of atherosclerosis, one of the most common vascular metabolic diseases (15, 16). Whether itaconate affects the progression of atherosclerosis is not known. Here, we show that Acod1 and itaconate attenuate atherogenesis by inducing an anti-inflammatory response via Nrf2. Overall, our work implicates the therapeutic potential of employing itaconate to treat atherosclerosis.

## Results

### Acod1 and itaconate accumulate during atherosclerosis

To determine if itaconate biosynthesis changes during atherogenesis, we examined the expression of Acod1 in mice with or without atherosclerosis. Briefly, we induced hypercholesterolemia and atherosclerosis by intraperitoneally injecting mice with an adeno-associated virus that overexpresses proprotein convertase subtilisin/kexin type 9 (AAV-PCSK9) and feeding them a western-diet (WD) for 10 weeks (17, 18). Non-atherosclerotic controls were administered vehicle and fed a standard laboratory chow diet.

We observed significantly increased levels of Acod1 mRNA and protein in the atherosclerotic aortas versus healthy control aortas (Figure 1A and 1B). Consistent with the elevated abundance of Acod1, atherosclerotic aortas accumulated more itaconate than controls ($p<0.0001$, Figure 1C). We examined other TCA cycle metabolites and found that isocitrate, malate, pyruvate and *cis*-aconitate were slightly but significantly

increased in atherosclerotic aorta, whereas α-ketoglutarate, succinate and citrate were mildly but not significantly affected (Figure 1C).

To investigate Acod1 levels during atherogenesis in human patients, we collected human atherosclerotic coronary arteries from a de-identified repository and performed immunohistochemistry (IHC). Intriguingly, a correlation analysis between the clinical occlusion percentage and the Acod1-positive area showed that the occlusion was significantly negatively correlated with Acod1 staining ($p<0.0001$, Figure 1D). These data suggest that Acod1 expression during atherogenesis mitigates occlusion.

Collectively, these results suggest that hypercholesterolemia and atherosclerosis lead to increased levels of Acod1 and itaconate, which in turn may help to attenuate atherogenesis.

**Acod1 deficiency exacerbates atherosclerosis in vivo**

To determine if Acod1 plays a role in atherogenesis, we examined *Acod1*$^{-/-}$ C57BL/6N mice before and during hypercholesterolemia (19, 20). We verified that Acod1 protein was not detected in *Acod1*$^{-/-}$ aortas (Supplemental Figure 1A), and itaconate levels did not increase with atherogenesis in *Acod1*$^{-/-}$ aortas (Supplemental Figure 1B).

WT and *Acod1*$^{-/-}$ mice displayed comparable plasma cholesterol levels throughout the hypercholesterolemia regimen (Supplemental Figure 2A). To investigate glucose metabolism, we performed glucose tolerance tests (GTT) and insulin tolerance tests

(ITT). *Acod1*$^{-/-}$ mice initially had lower glucose tolerance and insulin sensitivity than WT mice, however, hypercholesterolemia reduced the glucose tolerance and insulin sensitivity of WT mice over time, such that both genotypes displayed similarly compromised glucose metabolism from 3 weeks of hypercholesterolemia onwards (Supplemental Figure 2C). WT and *Acod1*$^{-/-}$ mice had similar body weights that increased due to hypercholesterolemia (Supplemental Figure 2D). Fat mass also increased with hypercholesterolemia, and although *Acod1*$^{-/-}$ mice initially had a higher fat mass than WT mice, this difference was eliminated after week 6 of hypercholesterolemia (Supplemental Figure 2D). WT and *Acod1*$^{-/-}$ mice had similar liver weights, gonadal white adipose tissue (GWAT) weights, liver lipid droplet accumulation and GWAT adipocyte sizes after 10 weeks of hypercholesterolemia (Supplemental Figure 2B). Importantly, hypercholesterolemia resulted in elevated levels of itaconate in the aortas of WT mice but not *Acod1*$^{-/-}$ mice ($p<0.0001$) (Supplemental Figure 2E).

We hypothesized that Acod1 and itaconate help to attenuate atherogenesis. Indeed, we observed larger atherosclerotic lesions in both the aortic root and brachiocephalic artery (BCA) of *Acod1*$^{-/-}$ mice compared to WT after 10 weeks of hypercholesterolemia (Figure 2A-C). Additionally, compared to atherosclerotic WT mice, atherosclerotic *Acod1*$^{-/-}$ mice exhibited a more than 3-fold increase in necrotic area in the aortic root (Figure 2A and 2C), a surrogate of plaque instability in the murine model of atherosclerosis (21).

Atherosclerotic progression involves dysfunctional turnover of the extracellular matrix, partly due to an imbalance of matrix metalloproteinases (MMPs) and tissue inhibitors of

metalloproteinases (TIMPs) (22). We examined the expression of select MMPs and TIMPs, and found that MMP9 and MMP12 were upregulated in atherosclerotic aortas from *Acod1*$^{-/-}$ mice versus WT, at both mRNA and protein levels (Supplemental Figure 3A and 3B). These MMPs have been found to promote plaque instability and increase atherosclerotic burden (22, 23), consistent with more severe atherogenesis in *Acod1*$^{-/-}$ mice versus WT.

**Acod1 deficiency increases inflammation during atherogenesis**

To determine if Acod1 deficiency affects inflammation in response to atherogenesis, we measured macrophage infiltration in the aorta, which is another surrogate marker of plaque instability (24). By IHC, we observed increased staining for the macrophage marker Mac2 in the aortic root and BCA of atherosclerotic *Acod1*$^{-/-}$ mice compared to WT (Figure 2D-F). In a complementary analysis, we enumerated macrophages and neutrophils via flow cytometry. Consistent with the observations above, the proportion and absolute number of macrophages were elevated in the atherosclerotic aorta of *Acod1*$^{-/-}$ compared to WT mice, whereas the proportion of neutrophils in the aorta was not affected (Supplemental Figure 4A). We infer that Acod1 deficiency increases macrophage infiltration in the aorta during atherogenesis.

Additionally, we measured circulating monocytes, which are a critical supply for atherosclerotic plaque macrophages (15, 25, 26), and circulating neutrophils, which are involved in monocyte recruitment (27). Intriguingly, we observed an increase in both peripheral neutrophils and peripheral monocytes (including the Ly6C$^{high}$ inflammatory

and Ly6C$^{low}$ patrolling subpopulations) in atherosclerotic *Acod1*$^{-/-}$ mice compared to WT (Supplemental Figure 4B). Notably, levels of peripheral neutrophils and monocytes were initially similar in *Acod1*$^{-/-}$ and WT mice, but both were increased in *Acod1*$^{-/-}$ mice compared to WT after 8-10 weeks of hypercholesterolemia, coincident with atherosclerosis (Supplemental Figure 4C). Thus, the absence of Acod1 during the development of atherosclerosis is associated with elevated levels of circulating neutrophils and monocytes.

To further investigate the impact of Acod1 deficiency on inflammation during atherogenesis, we measured the aortic gene expression of the following nine proinflammatory cytokines and chemokines that have been implicated in atherosclerosis: IL-1β, IL-6, IL-12, CCL2, CCL3, CCL5, CXCL1, CXCL2 and CXCL10 (25, 28, 29). All but IL-1β mRNA showed increased mRNA levels in atherosclerotic aorta from *Acod1*$^{-/-}$ compared to WT mice (Figure 2G). Furthermore, all nine corresponding proteins were secreted at higher levels in culture supernatant from atherosclerotic aortas of *Acod1*$^{-/-}$ compared to WT mice (Figure 2H). We also examined the anti-inflammatory cytokines IL-4, IL-10 and TGFβ (30-32). Both IL-4 and IL-10 were slightly but significantly increased in culture supernatant of atherosclerotic aorta from *Acod1*$^{-/-}$ mice compared to WT, whereas TGFβ isoforms were not significantly altered between genotypes (Supplemental Figure 4D).

Finally, we analyzed the expression of genes involved in the resolution of inflammation mediated by lipid mediators. We found that the expression of 12/15-lipoxygenase

(12/15-LO), which plays a protective role in atherogenesis (33), was decreased by ~50% in atherosclerotic aortas from *Acod1*$^{-/-}$ mice versus WT (Supplemental Figure 4E). In contrast, COX-2, which promotes atherogenesis (34), exhibited an approximately 3-fold increase in atherosclerotic aortas from *Acod1*$^{-/-}$ mice versus WT (Supplemental Figure 4E).

Taken together, our results indicate that constitutive genetic inactivation of *Acod1* exacerbates hypercholesterolemia-induced inflammation and atherogenesis, associated with increased lesion size, elevated macrophage infiltration, elevated peripheral neutrophils and monocytes, and higher expression of proinflammatory cytokines and chemokines.

**Acod1 deficiency promotes the proinflammatory polarization of macrophages during atherogenesis**

To determine how loss of Acod1 affects specific immune cell types during atherogenesis, we obtained plaque-containing atherosclerotic aorta tissues from WT and *Acod1*$^{-/-}$ mice and performed single cell RNA sequencing (scRNAseq). We detected many different types of immune cells and stromal cells (Supplemental Figure 5A), as expected.

Macrophages are a main constituent of atherosclerotic plaques and known to highly express *Acod1* (14, 35, 36), thus our initial analysis focused on this cell type. After quality control, we profiled 3050 WT and 3617 *Acod1*$^{-/-}$ macrophages, which is

comparable to previous single-cell studies on atherosclerotic macrophages (37, 38). Consistent with prior reports (37, 38), plaque macrophages exhibited strong heterogeneity that clustered into eight subsets (Cluster 0-7, abbreviated as c0-c7) (Figure 3A). Clusters c0, c5 and c1 were M1-like macrophages and generally expressed high levels of M1 markers such as Il-1β, Tnfα, Cxcl10 and/or Cd86 (Figure 3B and 3C). Clusters c3, c4 and c2, were M2-like macrophages and had high expression of typical M2 markers such as Trem2, Mrc1, Cd163 and/or Arg1 (Figure 3B and 3C). These six clusters were spread continuously on the UMAP (Figure 3A), suggesting a spectrum of macrophage activation status in vivo. The other two clusters, c6 and c7, were separated from the main populations and represented proliferating macrophages in G1 and G2/M phases, with low expression of M1 and M2 markers (Figure 3A-C). All eight clusters were present in both WT and *Acod1*$^{-/-}$ atherosclerotic aortas (Figure 3D).

Cluster c0 macrophages displayed unusually high cytokine and chemokine expression (i.e., Il-1β, Il-1α, Tnfα, Cxcl2, Cxcl1, Cxcl10, Ccl2, Ccl3, Ccl4, Ccl12, Cxcr4) compared to other clusters (Supplemental Table 1). This macrophage subset was previously described as "chemokine$^{hi}$ macrophages" (37) and "inflammatory macrophages" (38). Importantly, we detected a higher proportion of c0 M1-like macrophages in atherosclerotic plaques from *Acod1*$^{-/-}$ compared to WT mice (Figure 3E and 3F, Supplemental Table 2). In contrast, the proportion of c5 M1-like macrophages was decreased in *Acod1*$^{-/-}$ compared to WT plaques (Figure 3E and 3F, Supplemental Table 2). The c5 macrophages had a uniquely high type I interferon response (i.e., Ifit3, Ifit2, Ifit3b, Ifit1, Irf7, Ifi206, Ifi213, Ifi44, Ifi211, Ifi205, Ifi47, Ifi209, Isg15, Isg20), which

corresponded to “IFN signature$^{hi}$ macrophages” previously described (37). Type I interferon macrophages have been shown to exert both pro- and anti-inflammatory roles during atherosclerosis (39). The relative proportion of M2-like macrophages appeared roughly unchanged between WT and *Acod1*$^{-/-}$ (Figure 3E and 3F, Supplemental Table 2). Macrophage proliferation within plaques can contribute to atherosclerosis, especially at later stages (40-42), but the c7 (G2/M macrophages) was comparable between WT and *Acod1*$^{-/-}$ whereas c6 (G1 macrophages) was decreased in *Acod1*$^{-/-}$ atherosclerotic aortas (Figure 3E and 3F, Supplemental Table 2).

We determined the differentially expressed genes between macrophages from WT and *Acod1*$^{-/-}$ atherosclerotic aortas at the single cell level (Figure 3G-J, Supplemental Table 3). Consistent with the results above, genes encoding proinflammatory cytokines and chemokines, and inflammatory response-related genes, were upregulated in macrophages from *Acod1*$^{-/-}$ versus WT plaques, whereas type I interferon response genes were downregulated (Figure 3G-J, Supplemental Table 3). Collectively, these results suggest that Acod1 deficiency leads to an increased frequency of c0 M1-like macrophages with augmented proinflammatory polarization in atherosclerotic plaques.

We observed two subsets of monocytes in the atherosclerotic plaques, corresponding to classical Ly6c$^{high}$ and non-classical Ly6c$^{low}$ monocytes. Compared to WT, the aortic plaques from *Acod1*$^{-/-}$ mice had a higher proportion of Ly6c$^{low}$ monocytes (Supplemental Figure 5A-D), which could reflect an increased conversion of Ly6c$^{high}$ monocytes into inflammatory macrophages.

Consistent with other single cell RNAseq studies (43, 44), we detected several types of dendritic cells (DCs) (Supplemental Figure 5E-G). In addition, we also detected T and B lymphocytes, NK cells and type 2 innate lymphoid cells (ILC2) in atherosclerotic aortas. Interestingly, the proportion of mature/migratory DCs was increased in atherosclerotic aortas from *Acod1*$^{-/-}$ mice compared to WT (Supplemental Figure 5E-G). This DC subtype was shown to accumulate during advanced phase of atherosclerosis (44). Importantly, $CD8^+$ T cells displayed an increased frequency among T lymphocytes from *Acod1*$^{-/-}$ aortic plaques compared to WT (Supplemental Figure 5H-J), consistent with their role in promoting atherosclerosis (45, 46). Notably, many stress-related chaperones were upregulated on the single-cell level in DCs, T cells, B cells, and ILC2 from *Acod1*$^{-/-}$ atherosclerotic plaques compared to WT, whereas type II immune response genes were down-regulated in ILC2 and neutrophils from *Acod1*$^{-/-}$ plaques (Supplemental Figure 6, Supplemental Figure 7, Supplemental Table 4). Multiple inflammatory cytokines (CCL4, CCL5, CCL11, CXCL2, CXCL12) had elevated expression in fibroblasts from *Acod1*$^{-/-}$ plaques compared to WT (Supplemental Figure 8, Supplemental Table 4). Overall, these results are consistent with a highly inflammatory microenvironment in *Acod1*$^{-/-}$ atherosclerotic aortas.

**Acod1 in macrophages protects mice from atherogenesis**

To investigate the role of Acod1 in macrophages during atherogenesis, we used myeloid-specific Lysosomal-M (LysM)-Cre mice to generate conditional *Acod1* knockout mice (*Acod1*$^{fl/fl}$*LysM*$^{cre}$). We induced hypercholesterolemia and atherosclerosis in

*Acod1*$^{fl/fl}$*LysM*$^{cre}$ and in *Acod1*$^{fl/fl}$ littermate controls. We did not detect a difference in fasting cholesterol between atherosclerotic *Acod1*$^{fl/fl}$*LysM*$^{cre}$ and *Acod1*$^{fl/fl}$ mice (Supplemental Figure 9A). However, we observed a ~2-fold increase in the atherosclerotic lesion sizes in both the aortic root and BCA of *Acod1*$^{fl/fl}$*LysM*$^{cre}$ mice compared to control littermates, and an almost 3-fold increase in aortic root necrotic core size (Figure 4A-C). These increases are comparable to those caused by ubiquitous Acod1 deficiency (Figure 2A-C). Mac2 staining was also higher in both aortic root and BCA of atherosclerotic *Acod1*$^{fl/fl}$*LysM*$^{cre}$ mice compared to the *Acod1*$^{fl/fl}$ controls (Figure 4D-F). Relative to control *Acod1*$^{fl/fl}$ aortas, *Acod1*$^{fl/fl}$*LysM*$^{cre}$ aortas displayed increased infiltration of macrophages and increased expression of the macrophage markers F4/80, CD68 and CD64, whereas neutrophil infiltration and the levels of neutrophil markers like Mpo, Elane and S100a8 were unaltered (Supplemental Figure 9B and 9C). Taken together, we conclude that Acod1 in macrophages protects mice from atherogenesis during hypercholesterolemia.

**The itaconate derivative 4-ocytyl itaconate attenuates atherosclerosis, mitochondrial dysfunction and inflammation in WT mice**

4-ocytyl itaconate (OI) is an esterified derivative of itaconate that has been employed to mimic the in vivo biological effects of itaconate (14). To test the potential therapeutic efficacy of itaconate in atherosclerosis, we administered OI or vehicle via intraperitoneal injection twice per week for 10 weeks in WT mice with or without hypercholesterolemia. We found that the atherosclerotic lesion area, necrotic area, and Mac2-positive area within the aortic root and BCA were all reduced in atherosclerotic WT mice that received

OI versus vehicle (Figure 5). Thus, OI treatment attenuated atherogenesis caused by hypercholesterolemia in WT mice.

To confirm the effectiveness of OI, we analyzed mitochondrial function by performing a seahorse assay on peritoneal and aortic macrophages isolated from these four groups of mice. Compared to macrophages from healthy mice, those from atherosclerotic mice displayed an increased extracellular acidification rate (ECAR) and decreased oxygen consumption rate (OCR) (Supplemental Figure 10A), likely due to upregulated glycolysis (47). Notably, this compromise in mitochondrial function was significantly attenuated by OI treatment (Supplemental Figure 10A). We infer that OI treatment significantly inhibited the metabolic reprogramming and the shift from oxidative phosphorylation to glycolysis in macrophages during atherosclerosis. Moreover, we found that OI treatment attenuated the increased ROS production in macrophages during atherogenesis (Supplemental Figure 10B). These results are consistent with changes in cellular metabolism upon exposure to OI (12, 36, 48).

Moreover, OI treatment restored the levels of all nine proinflammatory cytokines and chemokines at the mRNA levels in atherosclerotic aortas of WT mice (Figure 6A), as well as at the protein level in the media of cultured atherosclerotic aortas (Figure 6B) and in plasma (Figure 6C). The levels of the anti-inflammatory cytokines IL-4, IL-10 and TGF$\beta$1 in atherosclerotic aortas were also restored by OI treatment of WT mice during atherogenesis (Supplemental Figure 11A). OI treatment reduced the expression of COX-2, chemokine like receptor 1 (Cmklr1) and formyl peptide receptor 2 (Fpr2) but

increased the expression of 12/15-LO in atherogenic aortas (Supplemental Figure 11B), consistent with their respective pro- or anti-inflammatory roles during the resolution of inflammation (33, 34, 49-51). OI treatment also suppressed the increased expression of MMP9, MMP12 and TIMP1 during atherogenesis (Supplemental Figure 11C and 11D). Thus, we conclude that treatment with the itaconate derivative OI diminishes atherosclerosis and inflammation in WT mice.

**Nrf2 is required for the itaconate-mediated inhibition of atherogenesis in mice**

Our results show that Acod1 in macrophages protects mice from atherogenesis. Given that itaconate activates Nrf2 signaling to protect against inflammation and oxidative stress in bone marrow-derived macrophages (BMDMs) and tissues (12, 52, 53), we hypothesized that Acod1 and itaconate inhibit atherogenesis and inflammation, at least in part, by activating Nrf2 signaling. To test this, first we measured Nrf2 protein levels in WT non-atherosclerotic and atherosclerotic aortas by western blot. Nrf2 protein levels were almost 3-fold higher in atherosclerotic versus non-atherosclerotic aorta in WT mice (Figure 7A), indicating that Nrf2 levels increase during atherogenesis. Compared to WT aortas, *Acod1*$^{-/-}$ aortas displayed reduced levels of Nrf2 protein, particularly after atherogenesis (Figure 7B). Intriguingly, WT mice treated with OI displayed elevated levels of Nrf2 protein in non-atherosclerotic and especially in atherosclerotic aortas (Figure 7C). Moreover, we observed a negative correlation between Nrf2 abundance and the extent of occlusion in human coronary arteries by IHC (Figure 7D), suggesting that Nrf2 inhibits atherogenesis.

To determine if Nrf2 helps to suppress atherogenesis mediated by Acod1 and itaconate, we examined *Nrf2*$^{-/-}$ mice. Atherogenesis was partially attenuated in *Nrf2*$^{-/-}$ mice compared to WT mice (Supplemental Figure 12), which is consistent with the phenotype observed in *ApoE*$^{-/-}$*Nrf2*$^{-/-}$ mice (54), probably due to the role of Nrf2 in CD36 expression and foam cell formation (54-56). Importantly, however, although OI treatment significantly ($p<0.0001$) decreased the lesion area and necrotic area in aortic root and BCA in WT mice, it had no impact on these phenotypes in *Nrf2*$^{-/-}$ mice (Supplemental Figure 12). We infer that Nrf2 is required for the itaconate-mediated suppression of atherogenesis in WT mice.

**Nrf2 contributes to the itaconate-mediated suppression of macrophage proinflammatory responses**

Nrf2 suppresses macrophage inflammatory responses (57). To investigate the role of Nrf2 in macrophages during atherogenesis, we calculated the activity of the Nrf2 signaling pathway in the scRNAseq dataset from WT and *Acod1*$^{-/-}$ atherosclerotic plaques. We used the UCell algorithm (58), which scores the relative gene expression of Nrf2 target genes in each cell. We found that Nrf2 activity was slightly but significantly lower in macrophages from *Acod1*$^{-/-}$ atherosclerotic plaques compared to WT counterparts (Supplemental Figure 13A). As expected, Nrf2 activity was higher in anti-inflammatory M2-like Trem2$^{hi}$ macrophages compared to the other macrophage subpopulations (Supplemental Figure 13B).

We further examined Nrf2 responses in BMDMs exposed to oxidized low-density lipoprotein cholesterol (oxLDL), a major activator of atherogenesis (59-61), and/or OI. We measured the expression of the Nrf2 target genes Hmox1, Nqo1 and Prdx1 and found that oxLDL induced the expression of Hmox1 and Nqo1 in WT BMDMs, with exposure to OI or OI+oxLDL resulting in even stronger upregulation of all three Nrf2 target genes (Supplemental Figure 14). Nrf2 target genes were not upregulated in *Nrf2*$^{-/-}$ BMDMs under any conditions (Supplemental Figure 14), as expected.

We next measured the gene expression of the nine proinflammatory cytokines and chemokines, and found that all except CXCL1 were significantly upregulated in WT BMDMs exposed to oxLDL, and OI treatment restored their expression (Figure 7E). Many of these genes were also induced in *Nrf2*$^{-/-}$ BMDMs exposed to oxLDL, but the rescue by OI treatment was attenuated (IL-12, CCL2 and CCL5) or eliminated (e.g. IL-1$\beta$, IL-6, CCL3, CXCL1, CXCL2 and CXCL10; Figure 7E). Similarly, the levels of secreted proinflammatory cytokines and chemokines were elevated in WT BMDMs exposed to oxLDL, and this proinflammatory effect was dampened by co-treatment with OI (Figure 7F). Again, exposing *Nrf2*$^{-/-}$ BMDMs to oxLDL also elevated the level of secreted proinflammatory cytokines and chemokines, but the rescue by OI treatment was attenuated or eliminated (Figure 7F). Similar to OI, itaconate (ITA) itself was also able to suppress oxLDL-mediated induction of the proinflammatory cytokines and chemokines (Supplemental Figure 15). We infer that itaconate activates Nrf2 in macrophages, which in turn mitigates a proinflammatory response.

## Discussion

Atherosclerosis is a chronic vascular disease that develops due to a failure to resolve inflammation within the arterial wall (62, 63). Typically, molecules that enhance the resolution of inflammation are lipid mediators (62-64), more specifically products derived from arachidonic acid, docosahexaenoic acid or eicosapentaenoic acid (62).

In our study, we found that the immunoregulatory byproduct of the TCA cycle, itaconate, increases within the arterial wall during atherogenesis. Loss of the enzyme that synthesizes itaconate, Acod1, promoted atherogenesis, whereas delivery of the itaconate derivative OI, which enhances the effect of itaconate, suppressed atherosclerosis in WT mice. Collectively, these results reveal that itaconate suppresses atherogenesis caused by hypercholesterolemia. Our work suggests that itaconate production in the myeloid lineage, including macrophages, contributes to suppressing atherogenesis. During atherosclerosis, itaconate activates Nrf2 which downregulates the expression and secretion of proinflammatory cytokines and chemokines, thus restraining macrophage infiltration and proinflammatory polarization.

Acod1 and itaconate were both increased in atherosclerotic aorta. Likewise, Acod1 and itaconate were also increased in ocular bacterial infection (52), and idiopathic pulmonary fibrosis (65) in mice. However, itaconate levels were lower in bronchoalveolar lavage from pulmonary fibrosis patients compared to healthy volunteers (65). We found that Acod1 levels negatively correlated with clinical occlusion of human coronary artery. Based on these data, we propose that inflammation initially

induces an anti-inflammatory response with subsequent itaconate production to dampen the inflammatory response. Pathogenesis arises both in experimental models and clinically when this anti-inflammatory response is compromised, leading to worsening inflammation. We found that administering the itaconate derivative OI diminished atherosclerotic lesions in mice, consistent with the protective role of itaconate in other inflammatory diseases (10, 12, 48, 52, 53). In the future, it would be interesting to examine if exogeneous itaconate administration reduces atherosclerosis, given the difference between itaconate and its derivatives (66).

We found that multiple proinflammatory cytokines and chemokines were downregulated by OI treatment but upregulated by Acod1 deficiency during atherosclerosis, which is consistent with their effects on atherogenesis and with other studies (10, 20, 48, 52, 67). OI treatment decreased the levels of inflammatory cytokines and chemokines not only in the aorta, but also systemically in plasma. Given that we administered OI systemically via intraperitoneal injection, it may target cells throughout the body and result in a systemic decrease in inflammation. Additionally, OI-mediated inhibition of inflammation and atherogenesis would in turn decrease the release of inflammatory cytokines and chemokines into the circulation. The protective roles of itaconate and its derivatives against inflammation are supported by other studies. For instance, the proinflammatory factors IL-1β, IL-6, IL-12, CCL2, CCL3, and CXCL1 were also increased in the lungs of *Acod1*$^{-/-}$ compared to WT mice after *M. tuberculosis* (*Mtb*) infection (20). Both IL-1β and IL-6 were increased by Acod1 deficiency, but decreased by OI treatment, in mouse retina during bacterial endophthalmitis (52). Serum (48) and peritoneal (10) IL-1β and

IL-6 were also reduced by OI treatment of a murine model of lethal endotoxemia and peritonitis. CXCL10 levels in culture supernatant were decreased by itaconate treatment of lung tissue after influenza infection (67). Overall, itaconate and its derivatives appear to be a potent anti-inflammatory therapeutic in multiple disease models.

Moreover, itaconate has been implicated to resolve inflammation. OI treatment of human BMDMs reduced COX-2 and MMP8 but increased TGFβ1, indicating that it promotes a wound-resolving phenotype (68). In our study, OI treatment of mice decreased COX-2, MMP8, MMP9 and MMP12 but increased 12/15-LO and TGFβ1, supporting a potential pro-resolving role in atherogenesis. Conversely, Acod1 deficiency resulted in decreased 12/15-LO, but increased COX-2, MMP8, MMP9 and MMP12. TGFβ1 did not show significant change in *Acod1*$^{-/-}$ mice, which may reflect a stronger effect of exogenous itaconate or its derivative compared to endogenous itaconate. Itaconate was also shown to drive the resolution of pulmonary fibrosis (69) and allergen-induced airway inflammation(70), underscoring the therapeutic potential of targeting this pathway.

Our results indicate that myeloid-specific expression of Acod1 protects mice from atherosclerosis, as *Acod1*$^{fl/fl}$*LysM*$^{cre}$ mice demonstrated aggravated atherogenesis compared to *Acod1*$^{fl/fl}$ control. Our single cell RNAseq data further reinforces the importance of macrophages in itaconate-mediated inflammatory blockade during atherogenesis. The c0 macrophage subset, named Cytokine$^{hi}$ M1-like macrophage, was significantly increased in *Acod1*$^{-/-}$ atherosclerotic aortas compared to WT. These

macrophages express high levels of proinflammatory cytokines and chemokines and their receptors including IL-1β, IL-1α, TNFα, CCL2, CCL3, CCL4, CCL12, CXCL1, CXCL2, CXCL10 and CXCR4. Similarly, Acod1 in peritoneal tissue-resident macrophages was shown to be a potential therapeutic target for peritoneal tumors, as specifically silencing *Acod1* in these cells reduces peritoneal tumor burden (71). In addition, adoptive transfer of WT but not *Acod1*$^{-/-}$ monocyte-derived airway macrophages into the airway of *Acod*$^{-/-}$ mice improved the outcome of bleomycin-induced pulmonary fibrosis (65), which further supports the importance of Acod1-expressing macrophages. As LysM is expressed in myeloid cells, including macrophages, developing a more specific Cre driver would help to precisely determine the exact identity of the itaconate-producing myeloid cells that suppress atherogenesis. More refined macrophage-specific Cre drivers are yet to be developed (72).

It should be noted that although macrophages are the primary contributor to itaconate-mediated atherosclerotic suppression, they are not the sole drivers of atherosclerosis. Endothelial cells, smooth muscle cells (SMCs), and other immune cells all play roles in atherosclerotic plaque formation and progression (73-75). Upon plaque initiation, lipids accumulate in the subendothelial region, leading to recruitment of classical monocytes and neutrophils (73, 76), where monocytes differentiate into macrophages. Macrophages are the most abundant immune cell subset in plaques, and they can also proliferate locally (42). During progression, SMCs migrate towards the developing fibrous cap, where they undergo clonal expansion (77). These cells interact with each other, both directly and indirectly, to control atherogenesis. For example, chemokines

such as CCL5 induce neutrophil recruitment, meanwhile, neutrophils themselves secrete chemoattractants like CCL2 and CCL5 to attract monocytes and activate macrophages (78). Activated SMCs also secrete chemokines to promote monocyte recruitment (73). Macrophages then secrete more inflammatory cytokines and chemokines to activate and induce neutrophils and SMCs migration. Activated T cells are also a substantial cell population in plaques (79) and play an overall pro-atherosclerotic role (80, 81). Our data support a model whereby macrophage-produced itaconate suppresses the production and secretion of proinflammatory cytokines and chemokines, which consequently dampens the migration and/or transformation of immune cells and stromal cells like SMCs and ultimately suppresses the monocyte/macrophage infiltration. Acod1 deficiency leads to increased proinflammatory polarization of macrophages, which contributes to a more inflammatory microenvironment such that other surrounding cell types likely also become more inflammatory, which in return reinforces the inflammatory profile of macrophages during atherogenesis. These different cell types form a network and collaborate to regulate anthogenesis.

There are multiple underlying mechanisms by which itaconate and its derivatives respond to inflammation, for example the IκBζ-ATF3 axis (82), succinate dehydrogenase inhibition (36) and Nrf2 activation (12). In our study, we found that Nrf2 levels increased with atherosclerosis, and that OI treatment enhanced this Nrf2 increase, whereas Acod1 deficiency caused Nrf2 levels to decrease. Subsequently, by comparing the responses of WT and *Nrf2*$^{-/-}$ BMDMs to oxLDL and/or OI in vitro and the

protective effect of OI in WT and *Nrf2*$^{-/-}$ mice in vivo, we demonstrated that Nrf2 is required for itaconate-mediated suppression of atherogenesis and inflammation. Our results are consistent with a potential therapeutic role of itaconate in ocular infection, which demonstrates that itaconate exerts an anti-inflammatory effect by potentiating Nrf2/HO1 signaling (52). Our results are also consistent with the recently reported mechanism through which itaconate improves donor heart preservation and function (53).

How itaconate regulates Nrf2 in atherosclerosis remains to be explored. The E3 ubiquitin ligase adaptor Kelch-like ECH-associated protein 1 (KEAP1) negatively regulates Nrf2 (83), and itaconate was recently shown to alkylate cysteine residues on KEAP1, allowing Nrf2 accumulation and activation of its downstream target genes, including anti-oxidant and anti-inflammatory genes (12). Itaconate may also increase oxidative phosphorylation during atherogenesis, which subsequently activates MAPK cascades that activate antioxidant response element (ARE) (84) and Nrf2 pathways (85-87). Indeed, *Acod1* knockdown significantly reduced MAPK phosphorylation in peritoneal tissue-resident macrophages in tumors (71). Furthermore, itaconate could activate Nrf2 through protein kinase R (PKR)-like endoplasmic reticulum kinase (PERK). Treating BMDMs with the itaconate derivative dimethyl itaconate led to increased PERK levels (82), and Nrf2 is known a direct substrate of PERK (88-90).

Itaconate and its derivatives also regulate immune responses independent of Nrf2. Dimethyl itaconate inhibits the IL-6-IκBζ axis via ATF3 independently of Nrf2 (82).

Furthermore, OI inhibited NLRP3 inflammasome activation in a Nrf2-independent manner (10). In addition, endogenous itaconate was not required for particulate matter-induced Nrf2 expression or inflammatory responses (91). During particulate matter-induced inflammation, endogenous itaconate, determined through the use of *Acod1*$^{-/-}$ mice, failed to activate Nrf2 in macrophages in vitro and in vivo (91), however Nrf2 protein levels were found reduced in *Acod1*$^{-/-}$ BMDMs (10, 82) and heart tissues (53) compared to WT. These results may indicate that the activation of Nrf2 by itaconate or its derivatives varies with inflammatory stimulus and the inflammatory microenvironment in vivo. Our in vitro results in BMDMs do not rule out the involvement of other signaling pathways in addition to Nrf2, which could potentially include ATF3-IκBζ pathway(82), NLRP3-NEK7 interaction and NLRP3 inflammasome(10), and targeting GAPDH and glycolysis (48, 92). Those additional potential mechanisms by which itaconate downregulates inflammation during atherogenesis will require future investigation.

In conclusion, our study has found an important role for the TCA metabolite itaconate in downregulating inflammation and suppressing atherogenesis, at least in part via activation of the antioxidant Nrf2 pathway. Our study provides impetus for developing therapeutics that boost itaconate pathways to reduce the burden of atherosclerosis.

## Methods

### Animal and Atherosclerosis

*Acod1*$^{-/-}$ mice were generated on C57BL/6N background, and they were acquired from Dr. Michael Diamond's laboratory located at Washington University, St. Louis, Missouri

(20). Wild type (WT) C57BL/6N mice (strain# 005304, Jackson Laboratory) were used as controls for *Acod1*$^{-/-}$ mice. *Acod1*$^{fl/fl}$ mice were also acquired from Dr. Michael Diamond's laboratory but on the C57BL/6 background. Myeloid-specific *Acod1* knockout (*Acod1*$^{fl/fl}$*LysM*$^{cre}$) mice were generated by crossing *Acod1*$^{fl/fl}$ mice with Cre-recombinase transgenic mice under the control of the Lysosomal-M promoter (LysM-Cre, strain# 004781, Jackson Laboratory) in Dr. Richard Mortensen's laboratory at the University of Michigan. Floxed littermates (*Acod1*$^{fl/fl}$) were used as controls for *Acod1*$^{fl/fl}$*LysM*$^{cre}$ mice. *Nrf2*$^{-/-}$ mice were originally purchased from Jackson Laboratory (strain# 017009) and then bred and housed in animal facility at the University of Michigan. WT C57BL/6 mice (strain# 000664, Jackson Laboratory) were used as controls for the *Nrf2*$^{-/-}$ mice. All mice were maintained on a 12-hour light-dark cycle with free access to food and water. All mice used in this study were 2-4 months old male mice unless specifically indicated. The numbers of mice for each experiment are shown in the figure legends.

To induce atherosclerosis, we used recombinant D377Y mPCSK9-AAV8 (PCSK9-AAV) that was generated at the University of Pennsylvania Vector Core. PCSK9-AAV was diluted in sterile saline and PCSK9-AAV ($5.0x10^9$ vector genomes/g) or vehicle was administered intraperitoneally. One week after the injection, mice were given western diet (WD, 42% calories from fat, Cat# TD.88137, formerly Envigo, now Inotivco Inc) for 10 weeks to increase cholesterol level and promote atherosclerosis. Week # in Supplemental Figure 2 and Supplemental Figure 4 indicates weeks after the initiation of the western diet. A standard laboratory diet (5L0D LabDiet) was used as a control diet. In a subset of mice, 4-Octyl itaconate (OI, 50mg/kg, Cat# SML2338, Sigma-Aldrich) in

40% cyclodextrin in PBS was administered twice per week intraperitoneally to mice since the initiation of the western diet. Mice were randomly assigned to treatment with OI or vehicle control.

**Histopathology**

Histology services were performed by the In Vivo Animal Core within the Unit for Laboratory Animal Medicine at the University of Michigan. Briefly, 10% formalin-fixed tissues were processed and embedded with paraffin. Tissues were then sectioned at 4μm thickness. Sectioning paradigms for mouse aortic root and brachiocephalic artery (BCA): aortic root, spanning approximately 250 μm, 24μm step levels and a total of 10 sections were collected beginning at the aortic valve leaflets; BCA, beginning at the proximal root of BCA, 100μm step levels and a total of 10 to 15 sections were collected until the right common carotid artery / right subclavian artery junction was reached. To determine the atherosclerotic lesion size and the acellular lesion (necrotic core) area (93-95), sections were subjected to hematoxylin and eosin (H&E) staining and then traced and measured using ImageJ. A total of 10 H&E-stained sections from aortic root and 10 to 15 H&E-stained sections from BCA were quantified per mouse. Immunohistochemical staining was performed to detect the macrophage marker Mac2 (sc-81728, Santa Cruz), and nucleus was counterstained with hematoxylin. For analysis of macrophages in aortic root, section #2, #4, #6, #8 and #10 were chosen.

**Human Samples**

Human coronary arteries were collected as part of an autopsy evaluation for use of the samples from a de-identified human repository for medical research. Following collections of the whole organ, coronary arteries were acquired and stored in 10% formalin indefinitely, then transferred to 70% ethanol, and 24 hours later processed and paraffin embedded for histological analysis. The human coronary artery samples were then sectioned and stained with anti-Acod1 (ab238580, Abcam) and anti-Nrf2 (ab31163, Abcam). The occlusion level was evaluated by the autopsy report as part of the cause of death analysis.

**Metabolomics**

Aortas were harvested, weighed and snap-frozen in liquid nitrogen, and then kept at −80 °C. Frozen aortas were homogenized with dry ice-cold 80% methanol followed by centrifugation at 10,000 × g for 5 min at 4 °C. The supernatant was collected and an aliquot of a volume equivalent to 10 mg of the tissue from each sample was saved at −80 °C. All aliquots were dried via speed vac for mass spectrometry processing. Agilent 1290 UHPLC system and Agilent Technologies Triple Quad 6470 Mass Spectrometer (LC-MS/MS) with a 1290 Infinity II LC Flexible Pump (Quaternary Pump), 1290 Infinity II Multisampler, and 1290 Infinity II Multicolumn Thermostat with a 6-port valve were used for metabolomics analysis. Data were collected using parameters published previously (96-98). Agilent MassHunter Workstation Software LC/MS Data Acquisition for 6400 Series Triple Quadrupole MS with Version B.08.02 was used for compound optimization and sample data acquisition. Agilent MassHunter Workstation Quantitative Analysis for

QQQ version 10.1, Build 10.1.733.0 was used to integrate and quantitate ion abundance peak areas. Absolute itaconate concentrations were calculated using an itaconate (93598, Sigma-Aldrich) standard curve.

**Single Cell RNA sequencing**

Aorta samples with atherosclerotic plaques from WT and *Acod1*$^{-/-}$ mice were analyzed by single cell RNA sequencing using the droplet-based 10X Genomics pipeline. Single cell suspensions from aortic root, ascending aorta and aortic arch, where most of the aortic plaques are, were prepared by mincing isolated tissues followed by enzymatic digestion with collagenase I (450 U/ml, LS004196, Worthington), collagenase XI (125 U/ml, C7657, Sigma-Aldrich), DNase I (60 U/ml, DN25, Sigma-Aldrich) and hyaluronidase (60 U/ml, H3506, Sigma-Aldrich) for 1 h at 37°C with agitation (99). Suspensions were then filtered, and dead cells were removed with a Dead Cell Removal Kit (480157, Biolegend) to improve cell viability of the samples. Cells were then washed, resuspended in RPMI 1640 + 10% fetal bovine serum and processed further by the Advanced Genomics Core at the University of Michigan. Single cells were partitioned into droplet emulsion using the Chromium Controller (10X Genomics, CA), where cells were lysed and cDNAs were reverse transcribed and barcoded. Amplified cDNAs were used to construct 5' gene expression (GEX) library. All cDNA libraries were sequenced on an Illumina NovaSeq-6000 platform with 150bp paired end reads. Raw reads were processed by the Cell Ranger pipeline and aligned to the mm10 reference genome (version: mm10-2020-A). Gene count matrices were generated and used for downstream bioinformatics analysis in the R 4.0.5 environment.

As a preprocessing step, ambient RNA contamination was removed by SoupX (100) which used empty droplets contained in the raw Cell Ranger output to calculate the profile of “soup” contamination. The corrected count matrices were then processed by the Seurat v4.1.0 package (101). Low quality cells were filtered out with the following criteria: the number of detected genes per cell should be greater than 200, the number of unique molecule identifiers (UMIs) should be less than 50,000, the percentage of expressed mitochondrial genes smaller than 10%, and the percentage of hemoglobin genes smaller than 3%. Raw counts were normalized with the “LogNormalize” method. Top 2,000 highly variable genes were scaled and used for principal component analysis (PCA). Samples were then integrated by the Harmony package (102) using the PCA result. The first 20 dimensions of the “harmony” reduction slot were used for constructing UMAP reduction and the shared nearest neighbor graph. The FindCluster function was used to identify clusters within the graph with a resolution of 0.4. Marker genes for each cluster were identified by the FindAllMarkers function using the default Wilcoxon Rank Sum test. Clusters were annotated using the SingleR package (103) with the mouse ImmGen dataset (104) as the reference, and then confirmed manually by searching top cluster-specific marker genes within Cellmarker 2.0 (105). To improve the resolution and accuracy of cell type assignment, a step-wise hierarchical annotation approach was adopted. For example, myeloid cells were subsetted out, re-integrated by Harmony and clustered again to annotate populations of macrophages, monocytes, neutrophils and dendritic cells. In a similar fashion, subpopulations of macrophages were annotated. The R package scProportionTest (106) was employed to assess

differences in subpopulation abundance within macrophages, monocytes, dendritic cells, and T cells between WT and *Acod1*$^{-/-}$, which calculates p values via permutation test and confidence intervals by bootstrapping. Differences in gene expression were determined using the FindMarkers function with default parameters. Genes with adjusted p-values < 0.05 and absolute values of fold change (FC) > 1.2 were considered differentially expressed and used for pathway enrichment analysis, which was performed using the enrichR package and the "GO_Biological_Process_2021" gene-set library (107).

To calculate Nrf2 activity score, a list of Nrf2 target genes was assembled from the literature: Hmox1, Nqo1, Pgd, Taldo1, G6pdx, Idh1, Gclm, Gclc, Gsr, Gpx1-4, Gsta1, Gsta2, Txn1, Txn2, Txnrd1, Txnip, Prdx1-6, Srxn1, Sod1, Sod2, Atf1, Ppp1r15b, Als2, Nfkbib, Nrf1, Cd36, Scarb1, Cox17, Cyp2a5, Abcc2-4, Akr1b3, Bcl2, Calcoco2, Areg, Cdkn2c, Fmo3, Keap1, Mcm7, Mdm2, Park7. This gene set was used as the input for the R package UCell (58) to evaluate the Nrf2 signature scores in each cell.

**Bone Marrow-Derived Macrophage**

Bone marrow-derived macrophages (BMDMs) were produced by flushing bone marrow from femurs and tibias. Briefly, bone marrow cells were flushed out with ice-cold PBS. After centrifugation, cells were resuspended in RPMI+ GlutaMax medium (61870, Gibco) supplemented with 10% fetal bovine serum, 30% L929-conditioned medium and 100 units/ml penicillin and streptomycin. The cells were then cultured in a humidified incubator under 95% air and 5% $CO_2$ at 37°C for 4 days. On day 4, the medium was

replaced by fresh medium. Two days later, BMDMs were differentiated and ready to use. BMDMs were treated by either OI (250 μM for 20h) alone, oxidized LDL (oxLDL, 100 μg/ml for 16h, Cat# L34357, ThermoFisher Scientific) alone, or OI plus oxLDL. OI was added 4 hs before oxLDL in the combined treatment. Vehicle was used as control. In another experiment, BMDMs were treated by itaconate (ITA, 7.5 mM for 20h, Cat# 93598, Sigma-Aldrich) and/or oxLDL (400 μg/ml for 16h).

**Quantitative RT-PCR**

Relative mRNA expression was determined using quantitative reverse-transcription polymerase chain reaction (qRT-PCR). Total RNA was extracted using TRIzol reagent and RNA was reverse transcribed to cDNA. Quantitative PCR was performed using a 7900HT fast real-time PCR system (Applied Biosystems) and relative mRNA level was analyzed using the comparative method and normalized to the internal control, L32. Primer sequences for qRT-PCR are shown in Supplemental Table 5.

**Western Blot**

Aorta was harvested and snap-frozen in liquid nitrogen. Protein extraction was then performed by homogenizing the frozen aorta in lysis buffer (78510, Thermofisher Scientific) with 1% protease inhibitor cocktail (P8340, Sigma-Aldrich) and 1% phosphatase inhibitor cocktail (P5726, Sigma-Aldrich). Tissue lysates were electrophoresed on 10% SDS-polyacrylamide gels (NP0315BOX, Invitrogen) and transferred to PVDF membranes (IB401001, ThermoFisher Scienfic). Blots were blocked in 5% BSA in PBST (1% Tween-20 in PBS) for 1 h at room temperature (RT) or

4 °C overnight. Membranes were then incubated for 1 h at RT with primary antibodies against Acod1 (ab222411, Abcam), Nrf2 (12721, Cell Signaling Technology) or GAPDH (2118S, Cell Signaling Technology). After washing, membranes were incubated with secondary antibodies for 30min and then illuminated with chemiluminescent substrate (34577, ThermoFisher Scientific) using a BioRad ChemiDoc (Hercules, CA, USA).

**Multiplex Assay and ELISA**

V-PLEX, U-PLEX and R-PLEX assays from MSD (Meso Scale Discovery) multi-spot assay system were used to quantify proteins in aorta tissue culture medium, BMDMs culture medium and plasma. Customized panels were used according to the manufacturer's instructions. V-PLEX Panel 1 (K15048D) includes IL-1β, IL-4, IL-6, IL-10, IL-12 and CXCL1. V-PLEX Panel 2 (K15245D) includes CCL2, CCL3, CXCL2 and CXCL10. CCL5 (K152A2K-1), TGFβ Combo (K15242K-1) and MMP9 (B22ZG-2) were measured by U-PLEX assay. TIMP1 (F22YO-3) was measured by R-PLEX assay. MMP12 was measured by ELISA (ab213878, Abcam) according to the manufacturer's instructions.

**Statistical Analysis**

Unpaired two-tailed Student's t-test, 2-way ANOVA followed by Tukey's post hoc test, and two-sided Pearson correlation test were used for statistical analysis. Figures that used 2-way ANOVA, p values indicate the main effect between the indicated groups. All statistical analysis was performed in GraphPad Prism (GraphPad Software, Inc). $p<0.05$ was considered significant.

## Study approval

Animal protocols were approved by the University of Michigan Animal Care and Use Committee. All animal procedures were performed in accordance with the Guide for Care and Use of Laboratory Animals and conformed to the NIH guidelines. Human samples were collected from a de-identified human repository for medical research. As the samples were de-identified, IRB was not required.

## Data availability

Raw and processed mouse single-cell RNA sequencing data have been deposited in the NCBI GEO database under the identifier GSE235749 (https://www.ncbi.nlm.nih.gov/geo/query/acc.cgi?acc=GSE235749).
All remaining data that support the findings of this study are available in the main text or the supplemental materials. Supporting data values are shown in the file named Numerical data for all figures.

## Author contributions

JS and YZ designed, conducted experiments, analyzed data, and wrote the manuscript. RAF, AA, SW and PS provided resources and performed experimental work. DJT, JCD, CAL, RMM and MS provided critical materials, guidance, and comments. DRG designed, directed, supervised the study, and wrote the manuscript. All authors reviewed the manuscript and provided final approval for submission. The order of co-first authors was based on the order that they joined the project.

## Acknowledgments

This study was supported by National Institute of Health (NIH) awards AI138347, AG028082 and HL155169 to DRG, in addition to an American Heart Association award 898210 to JS. YZ was supported by the National Natural Science Foundation of China (31401220, 31571465) and the Natural Science Foundation of Jiangsu Province (BK20211312). We acknowledge Wendy Rosebury-Smith in the In Vivo Animal Core at the University of Michigan for her expertise and assistance with histopathology. For single-cell RNA sequencing, the sequencing was performed in the Advanced Genomics Core at the University of Michigan.

## Disclosure

The authors declare no conflict of interest.

## References

1. Strelko CL, Lu W, Dufort FJ, Seyfried TN, Chiles TC, Rabinowitz JD, et al. Itaconic acid is a mammalian metabolite induced during macrophage activation. *J Am Chem Soc.* 2011;133(41):16386-9.
2. Michelucci A, Cordes T, Ghelfi J, Pailot A, Reiling N, Goldmann O, et al. Immune-responsive gene 1 protein links metabolism to immunity by catalyzing itaconic acid production. *Proc Natl Acad Sci U S A.* 2013;110(19):7820-5.
3. Bambouskova M, Gorvel L, Lampropoulou V, Sergushichev A, Loginicheva E, Johnson K, et al. Electrophilic properties of itaconate and derivatives regulate the IκBζ–ATF3 inflammatory axis. *Nature.* 2018;556(7702):501-4.
4. Lampropoulou V, Sergushichev A, Bambouskova M, Nair S, Emma, Loginicheva E, et al. Itaconate Links Inhibition of Succinate Dehydrogenase with Macrophage Metabolic Remodeling and Regulation of Inflammation. *Cell Metabolism.* 2016;24(1):158-66.
5. Cordes T, Lucas A, Divakaruni AS, Murphy AN, Cabrales P, and Metallo CM. Itaconate modulates tricarboxylic acid and redox metabolism to mitigate reperfusion injury. *Molecular Metabolism.* 2020;32:122-35.

6. Ogger PP, Albers GJ, Hewitt RJ, O'Sullivan BJ, Powell JE, Calamita E, et al. Itaconate controls the severity of pulmonary fibrosis. *Science Immunology.* 2020;5(52):eabc1884.
7. Song H, Xu T, Feng X, Lai Y, Yang Y, Zheng H, et al. Itaconate prevents abdominal aortic aneurysm formation through inhibiting inflammation via activation of Nrf2. *EBioMedicine.* 2020;57:102832.
8. Chen YJ, Li GN, Li XJ, Wei LX, Fu MJ, Cheng ZL, et al. Targeting IRG1 reverses the immunosuppressive function of tumor-associated macrophages and enhances cancer immunotherapy. *Sci Adv.* 2023;9(17):eadg0654.
9. Duan X, Hu M, Yang L, Zhang S, Wang B, Li T, et al. IRG1 prevents excessive inflammatory responses and cardiac dysfunction after myocardial injury. *Biochem Pharmacol.* 2023;213:115614.
10. Hooftman A, Angiari S, Hester S, Corcoran SE, Runtsch MC, Ling C, et al. The Immunomodulatory Metabolite Itaconate Modifies NLRP3 and Inhibits Inflammasome Activation. *Cell Metab.* 2020;32(3):468-78 e7.
11. Zheng D, Liwinski T, and Elinav E. Inflammasome activation and regulation: toward a better understanding of complex mechanisms. *Cell Discov.* 2020;6:36.
12. Mills EL, Ryan DG, Prag HA, Dikovskaya D, Menon D, Zaslona Z, et al. Itaconate is an anti-inflammatory metabolite that activates Nrf2 via alkylation of KEAP1. *Nature.* 2018;556(7699):113-7.
13. Ma Q. Role of nrf2 in oxidative stress and toxicity. *Annu Rev Pharmacol Toxicol.* 2013;53:401-26.
14. Peace CG, and O'Neill LAJ. The role of itaconate in host defense and inflammation. *Journal of Clinical Investigation.* 2022;132(2).
15. Moore KJ, Sheedy FJ, and Fisher EA. Macrophages in atherosclerosis: a dynamic balance. *Nat Rev Immunol.* 2013;13(10):709-21.
16. Karlinsey K, Qu L, Matz AJ, and Zhou B. A novel strategy to dissect multifaceted macrophage function in human diseases. *Journal of Leukocyte Biology.* 2022;112(6):1535-42.
17. Bjorklund MM, Hollensen AK, Hagensen MK, Dagnaes-Hansen F, Christoffersen C, Mikkelsen JG, et al. Induction of atherosclerosis in mice and hamsters without germline genetic engineering. *Circ Res.* 2014;114(11):1684-9.
18. Tyrrell DJ, Blin M, Song J, Wood S, Zhang M, Beard DA, et al. Age-Associated Mitochondrial Dysfunction Accelerates Atherogenesis. *Circulation Research.* 2020;126:298–314.
19. Frieler RA, Vigil TM, Song J, Leung C, Goldstein DR, Lumeng CN, et al. Aconitate decarboxylase 1 regulates glucose homeostasis and obesity in mice. *Obesity.* 2022;30(9):1818-30.
20. Nair S, Huynh JP, Lampropoulou V, Loginicheva E, Esaulova E, Gounder AP, et al. Irg1 expression in myeloid cells prevents immunopathology during M. tuberculosis infection. *J Exp Med.* 2018;215(4):1035-45.
21. Caulin C, Nguyen T, Lang GA, Goepfert TM, Brinkley BR, Cai W-W, et al. An inducible mouse model for skin cancer reveals distinct roles for gain- and loss-of-function p53 mutations. *The Journal of Clinical Investigation.* 2007;117(7):1893-901.

22. Kremastiotis G, Handa I, Jackson C, George S, and Johnson J. Disparate effects of MMP and TIMP modulation on coronary atherosclerosis and associated myocardial fibrosis. *Sci Rep.* 2021;11(1):23081.
23. Basiak M, Hachula M, Kosowski M, Machnik G, Maliglowka M, Dziubinska-Basiak M, et al. The Effect of PCSK9 Inhibition on the Stabilization of Atherosclerotic Plaque Determined by Biochemical and Diagnostic Imaging Methods. *Molecules.* 2023;28(15).
24. Fernandez-Hernando C, Ackah E, Yu J, Suarez Y, Murata T, Iwakiri Y, et al. Loss of Akt1 Leads to Severe Atherosclerosis and Occlusive Coronary Artery Disease. *Cell Metabolism.* 2007;6(6):446-57.
25. Gautier E, Jakubzick C, and Randolph G. Regulation of the migration and survival of monocyte subsets by chemokine receptors and its relevance to atherosclerosis. *Arterioscler Thromb Vasc Biol.* 2009;29:1412 - 8.
26. Flynn MC, Pernes G, Lee MKS, Nagareddy PR, and Murphy AJ. Monocytes, Macrophages, and Metabolic Disease in Atherosclerosis. *Front Pharmacol.* 2019;10:666.
27. Soehnlein O, Lindbom L, and Weber C. Mechanisms underlying neutrophil-mediated monocyte recruitment. *Blood.* 2009;114(21):4613-23.
28. Tyrrell DJ, and Goldstein DR. Ageing and atherosclerosis: vascular intrinsic and extrinsic factors and potential role of IL-6. *Nature Reviews Cardiology.* 2021;18(1):58-68.
29. Ramji DP, and Davies TS. Cytokines in atherosclerosis: Key players in all stages of disease and promising therapeutic targets. *Cytokine Growth Factor Rev.* 2015;26(6):673-85.
30. Chen H, Li D, Saldeen T, and Mehta JL. Transforming growth factor-beta(1) modulates oxidatively modified LDL-induced expression of adhesion molecules: role of LOX-1. *Circ Res.* 2001;89(12):1155-60.
31. DiChiara MR, Kiely JM, Gimbrone MA, Jr., Lee ME, Perrella MA, and Topper JN. Inhibition of E-selectin gene expression by transforming growth factor beta in endothelial cells involves coactivator integration of Smad and nuclear factor kappaB-mediated signals. *J Exp Med.* 2000;192(5):695-704.
32. Feinberg MW, Jain MK, Werner F, Sibinga NE, Wiesel P, Wang H, et al. Transforming growth factor-beta 1 inhibits cytokine-mediated induction of human metalloelastase in macrophages. *J Biol Chem.* 2000;275(33):25766-73.
33. Merched AJ, Ko K, Gotlinger KH, Serhan CN, and Chan L. Atherosclerosis: evidence for impairment of resolution of vascular inflammation governed by specific lipid mediators. *FASEB J.* 2008;22(10):3595-606.
34. Burleigh ME, Babaev VR, Oates JA, Harris RC, Gautam S, Riendeau D, et al. Cyclooxygenase-2 promotes early atherosclerotic lesion formation in LDL receptor-deficient mice. *Circulation.* 2002;105(15):1816-23.
35. Hall CJ, Boyle RH, Astin JW, Flores MV, Oehlers SH, Sanderson LE, et al. Immunoresponsive gene 1 augments bactericidal activity of macrophage-lineage cells by regulating beta-oxidation-dependent mitochondrial ROS production. *Cell Metab.* 2013;18(2):265-78.
36. Lampropoulou V, Sergushichev A, Bambouskova M, Nair S, Vincent EE, Loginicheva E, et al. Itaconate Links Inhibition of Succinate Dehydrogenase with

Macrophage Metabolic Remodeling and Regulation of Inflammation. *Cell Metab.* 2016;24(1):158-66.
37. Lin JD, Nishi H, Poles J, Niu X, McCauley C, Rahman K, et al. Single-cell analysis of fate-mapped macrophages reveals heterogeneity, including stem-like properties, during atherosclerosis progression and regression. *JCI Insight.* 2019;4(4).
38. Cochain C, Vafadarnejad E, Arampatzi P, Pelisek J, Winkels H, Ley K, et al. Single-Cell RNA-Seq Reveals the Transcriptional Landscape and Heterogeneity of Aortic Macrophages in Murine Atherosclerosis. *Circ Res.* 2018;122(12):1661-74.
39. Chen HJ, Tas SW, and de Winther MPJ. Type-I interferons in atherosclerosis. *The Journal of experimental medicine.* 2020;217(1).
40. Spann NJ, Garmire LX, McDonald JG, Myers DS, Milne SB, Shibata N, et al. Regulated accumulation of desmosterol integrates macrophage lipid metabolism and inflammatory responses. *Cell.* 2012;151(1):138-52.
41. Rosenfeld ME. Macrophage proliferation in atherosclerosis: an historical perspective. *Arterioscler Thromb Vasc Biol.* 2014;34(10):e21-2.
42. Robbins CS, Hilgendorf I, Weber GF, Theurl I, Iwamoto Y, Figueiredo JL, et al. Local proliferation dominates lesional macrophage accumulation in atherosclerosis. *Nat Med.* 2013;19(9):1166-72.
43. Jung SH, Hwang BH, Shin S, Park EH, Park SH, Kim CW, et al. Spatiotemporal dynamics of macrophage heterogeneity and a potential function of Trem2(hi) macrophages in infarcted hearts. *Nature communications.* 2022;13(1):4580.
44. Zernecke A, Erhard F, Weinberger T, Schulz C, Ley K, Saliba AE, et al. Integrated single-cell analysis-based classification of vascular mononuclear phagocytes in mouse and human atherosclerosis. *Cardiovascular research.* 2023;119(8):1676-89.
45. Schäfer S, and Zernecke A. CD8(+) T Cells in Atherosclerosis. *Cells.* 2020;10(1).
46. Cochain C, Koch M, Chaudhari SM, Busch M, Pelisek J, Boon L, et al. CD8+ T Cells Regulate Monopoiesis and Circulating Ly6C-high Monocyte Levels in Atherosclerosis in Mice. *Circ Res.* 2015;117(3):244-53.
47. Li L, Wang M, Ma Q, Ye J, and Sun G. Role of glycolysis in the development of atherosclerosis. *Am J Physiol Cell Physiol.* 2022;323(2):C617-C29.
48. Liao ST, Han C, Xu DQ, Fu XW, Wang JS, and Kong LY. 4-Octyl itaconate inhibits aerobic glycolysis by targeting GAPDH to exert anti-inflammatory effects. *Nat Commun.* 2019;10(1):5091.
49. Ye RD, Boulay F, Wang JM, Dahlgren C, Gerard C, Parmentier M, et al. International Union of Basic and Clinical Pharmacology. LXXIII. Nomenclature for the formyl peptide receptor (FPR) family. *Pharmacol Rev.* 2009;61(2):119-61.
50. Xie Y, Huang Y, Ling X, Qin H, Wang M, and Luo B. Chemerin/CMKLR1 Axis Promotes Inflammation and Pyroptosis by Activating NLRP3 Inflammasome in Diabetic Cardiomyopathy Rat. *Front Physiol.* 2020;11:381.
51. Yun H, Dumbell R, Hanna K, Bowen J, McLean SL, Kantamneni S, et al. The Chemerin-CMKLR1 Axis is Functionally important for Central Regulation of Energy Homeostasis. *Front Physiol.* 2022;13:897105.

52. Singh S, Singh PK, Jha A, Naik P, Joseph J, Giri S, et al. Integrative metabolomics and transcriptomics identifies itaconate as an adjunct therapy to treat ocular bacterial infection. *Cell Rep Med.* 2021;2(5):100277.
53. Lei I, Huang W, Noly PE, Naik S, Ghali M, Liu L, et al. Metabolic reprogramming by immune-responsive gene 1 up-regulation improves donor heart preservation and function. *Sci Transl Med.* 2023;15(682):eade3782.
54. Sussan TE, Jun J, Thimmulappa R, Bedja D, Antero M, Gabrielson KL, et al. Disruption of Nrf2, a key inducer of antioxidant defenses, attenuates ApoE-mediated atherosclerosis in mice. *PLoS One.* 2008;3(11):e3791.
55. Hopkins PN. Molecular biology of atherosclerosis. *Physiol Rev.* 2013;93(3):1317-542.
56. Alonso-Pineiro JA, Gonzalez-Rovira A, Sanchez-Gomar I, Moreno JA, and Duran-Ruiz MC. Nrf2 and Heme Oxygenase-1 Involvement in Atherosclerosis Related Oxidative Stress. *Antioxidants (Basel).* 2021;10(9).
57. Kobayashi EH, Suzuki T, Funayama R, Nagashima T, Hayashi M, Sekine H, et al. Nrf2 suppresses macrophage inflammatory response by blocking proinflammatory cytokine transcription. *Nat Commun.* 2016;7:11624.
58. Andreatta M, and Carmona SJ. UCell: Robust and scalable single-cell gene signature scoring. *Computational and structural biotechnology journal.* 2021;19:3796-8.
59. Grootaert MO, da Costa Martins PA, Bitsch N, Pintelon I, De Meyer GR, Martinet W, et al. Defective autophagy in vascular smooth muscle cells accelerates senescence and promotes neointima formation and atherogenesis. *Autophagy.* 2015;11(11):2014-32.
60. Sergin I, Bhattacharya S, Emanuel R, Esen E, Stokes CJ, Evans TD, et al. Inclusion bodies enriched for p62 and polyubiquitinated proteins in macrophages protect against atherosclerosis. *Sci Signal.* 2016;9(409):ra2.
61. Steinbrecher UP, Witztum JL, Parthasarathy S, and Steinberg D. Decrease in reactive amino groups during oxidation or endothelial cell modification of LDL. Correlation with changes in receptor-mediated catabolism. *Arteriosclerosis.* 1987;7(2):135-43.
62. Doran AC. Inflammation Resolution: Implications for Atherosclerosis. *Circulation Research.* 2022;130(1):130-48.
63. Arnardottir H, Thul S, Pawelzik S-C, Karadimou G, Artiach G, Gallina AL, et al. The resolvin D1 receptor GPR32 transduces inflammation resolution and atheroprotection. *Journal of Clinical Investigation.* 2021;131(24).
64. Serhan CN, Chiang N, and Van Dyke T. Resolving inflammation: dual anti-inflammatory and pro-resolution lipid mediators. *Nat Rev Immunol.* 2008;8:349-61.
65. Ogger PP, Albers GJ, Hewitt RJ, O'Sullivan BJ, Powell JE, Calamita E, et al. Itaconate controls the severity of pulmonary fibrosis. *Sci Immunol.* 2020;5(52).
66. Swain A, Bambouskova M, Kim H, Andhey PS, Duncan D, Auclair K, et al. Comparative evaluation of itaconate and its derivatives reveals divergent inflammasome and type I interferon regulation in macrophages. *Nat Metab.* 2020;2(7):594-602.

67. Sohail A, Iqbal AA, Sahini N, Chen F, Tantawy M, Waqas SFH, et al. Itaconate and derivatives reduce interferon responses and inflammation in influenza A virus infection. *PLoS Pathog.* 2022;18(1):e1010219.
68. Maassen S, Coenen B, Ioannidis M, Harber K, Grijpstra P, Van den Bossche J, et al. Itaconate promotes a wound resolving phenotype in pro-inflammatory macrophages. *Redox Biol.* 2023;59:102591.
69. P Ogger PG, R J Hewitt, P L Molyneaux, T M Maher, C M Lloyd, A J Byrne. Itaconate drives the resolution of pulmonary fibrosis. *ERJ Open Research.* 2020;6:72.
70. Jaiswal AK, Yadav J, Makhija S, Mazumder S, Mitra AK, Suryawanshi A, et al. Irg1/itaconate metabolic pathway is a crucial determinant of dendritic cells immune-priming function and contributes to resolute allergen-induced airway inflammation. *Mucosal Immunol.* 2022;15(2):301-13.
71. Weiss JM, Davies LC, Karwan M, Ileva L, Ozaki MK, Cheng RY, et al. Itaconic acid mediates crosstalk between macrophage metabolism and peritoneal tumors. *J Clin Invest.* 2018;128(9):3794-805.
72. Shi J, Hua L, Harmer D, Li P, and Ren G. Cre Driver Mice Targeting Macrophages. *Methods Mol Biol.* 2018;1784:263-75.
73. Soehnlein O, and Libby P. Targeting inflammation in atherosclerosis - from experimental insights to the clinic. *Nat Rev Drug Discov.* 2021;20(8):589-610.
74. Gimbrone MA, Jr., and Garcia-Cardena G. Endothelial Cell Dysfunction and the Pathobiology of Atherosclerosis. *Circ Res.* 2016;118(4):620-36.
75. Gistera A, and Hansson GK. The immunology of atherosclerosis. *Nat Rev Nephrol.* 2017;13(6):368-80.
76. Combadiere C, Potteaux S, Rodero M, Simon T, Pezard A, Esposito B, et al. Combined inhibition of CCL2, CX3CR1, and CCR5 abrogates Ly6C(hi) and Ly6C(lo) monocytosis and almost abolishes atherosclerosis in hypercholesterolemic mice. *Circulation.* 2008;117(13):1649-57.
77. Misra A, Feng Z, Chandran RR, Kabir I, Rotllan N, Aryal B, et al. Integrin beta3 regulates clonality and fate of smooth muscle-derived atherosclerotic plaque cells. *Nat Commun.* 2018;9(1):2073.
78. Bentzon JF, Otsuka F, Virmani R, and Falk E. Mechanisms of plaque formation and rupture. *Circ Res.* 2014;114(12):1852-66.
79. Hansson GK, Holm J, and Jonasson L. Detection of activated T lymphocytes in the human atherosclerotic plaque. *Am J Pathol.* 1989;135(1):169-75.
80. Paulsson G, Zhou X, Tornquist E, and Hansson GK. Oligoclonal T cell expansions in atherosclerotic lesions of apolipoprotein E-deficient mice. *Arterioscler Thromb Vasc Biol.* 2000;20(1):10-7.
81. Zhou X, Nicoletti A, Elhage R, and Hansson GK. Transfer of CD4(+) T cells aggravates atherosclerosis in immunodeficient apolipoprotein E knockout mice. *Circulation.* 2000;102(24):2919-22.
82. Bambouskova M, Gorvel L, Lampropoulou V, Sergushichev A, Loginicheva E, Johnson K, et al. Electrophilic properties of itaconate and derivatives regulate the IkappaBzeta-ATF3 inflammatory axis. *Nature.* 2018;556(7702):501-4.

83. Wakabayashi N, Itoh K, Wakabayashi J, Motohashi H, Noda S, Takahashi S, et al. Keap1-null mutation leads to postnatal lethality due to constitutive Nrf2 activation. *Nat Genet.* 2003;35(3):238-45.
84. Kong AN, Owuor E, Yu R, Hebbar V, Chen C, Hu R, et al. Induction of xenobiotic enzymes by the MAP kinase pathway and the antioxidant or electrophile response element (ARE/EpRE). *Drug Metab Rev.* 2001;33(3-4):255-71.
85. Zipper LM, and Mulcahy RT. Inhibition of ERK and p38 MAP kinases inhibits binding of Nrf2 and induction of GCS genes. *Biochem Biophys Res Commun.* 2000;278(2):484-92.
86. Huang HC, Nguyen T, and Pickett CB. Regulation of the antioxidant response element by protein kinase C-mediated phosphorylation of NF-E2-related factor 2. *Proc Natl Acad Sci U S A.* 2000;97(23):12475-80.
87. Zipper LM, and Mulcahy RT. Erk activation is required for Nrf2 nuclear localization during pyrrolidine dithiocarbamate induction of glutamate cysteine ligase modulatory gene expression in HepG2 cells. *Toxicol Sci.* 2003;73(1):124-34.
88. Cullinan SB, Zhang D, Hannink M, Arvisais E, Kaufman RJ, and Diehl JA. Nrf2 is a direct PERK substrate and effector of PERK-dependent cell survival. *Mol Cell Biol.* 2003;23(20):7198-209.
89. Cullinan SB, and Diehl JA. PERK-dependent activation of Nrf2 contributes to redox homeostasis and cell survival following endoplasmic reticulum stress. *J Biol Chem.* 2004;279(19):20108-17.
90. Mimura J, and Itoh K. Role of Nrf2 in the pathogenesis of atherosclerosis. *Free Radic Biol Med.* 2015;88(Pt B):221-32.
91. Sun KA, Li Y, Meliton AY, Woods PS, Kimmig LM, Cetin-Atalay R, et al. Endogenous itaconate is not required for particulate matter-induced NRF2 expression or inflammatory response. *Elife.* 2020;9.
92. Blatnik M, Frizzell N, Thorpe SR, and Baynes JW. Inactivation of glyceraldehyde-3-phosphate dehydrogenase by fumarate in diabetes: formation of S-(2-succinyl)cysteine, a novel chemical modification of protein and possible biomarker of mitochondrial stress. *Diabetes.* 2008;57(1):41-9.
93. Paigen B, Morrow A, Holmes PA, Mitchell D, and Williams RA. Quantitative assessment of atherosclerotic lesions in mice. *Atherosclerosis.* 1987;68:231-40.
94. Fernandez-Hernando C, Ackah E, Yu J, Suarez Y, Murata T, Iwakiri Y, et al. Loss of Akt1 leads to severe atherosclerosis and occlusive coronary artery disease. *Cell Metab.* 2007;6(6):446-57.
95. Daugherty A, Tall Alan R, Daemen Mat JAP, Falk E, Fisher Edward A, García-Cardeña G, et al. Recommendation on Design, Execution, and Reporting of Animal Atherosclerosis Studies: A Scientific Statement From the American Heart Association. *Arteriosclerosis, Thrombosis, and Vascular Biology.* 2017;37(9):e131-e57.
96. Halbrook CJ, Thurston G, Boyer S, Anaraki C, Jimenez JA, McCarthy A, et al. Differential integrated stress response and asparagine production drive symbiosis and therapy resistance of pancreatic adenocarcinoma cells. *Nat Cancer.* 2022;3(11):1386-403.

97. Hong HS, Mbah NE, Shan M, Loesel K, Lin L, Sajjakulnukit P, et al. OXPHOS promotes apoptotic resistance and cellular persistence in T(H)17 cells in the periphery and tumor microenvironment. *Sci Immunol.* 2022;7(77):eabm8182.
98. Kerk SA, Lin L, Myers AL, Sutton DJ, Andren A, Sajjakulnukit P, et al. Metabolic requirement for GOT2 in pancreatic cancer depends on environmental context. *Elife.* 2022;11.
99. Hu D, Yin C, Mohanta SK, Weber C, and Habenicht AJ. Preparation of Single Cell Suspensions from Mouse Aorta. *Bio-protocol.* 2016;6(11).
100. Young MD, and Behjati S. SoupX removes ambient RNA contamination from droplet-based single-cell RNA sequencing data. *GigaScience.* 2020;9(12).
101. Hao Y, Hao S, Andersen-Nissen E, Mauck WM, 3rd, Zheng S, Butler A, et al. Integrated analysis of multimodal single-cell data. *Cell.* 2021;184(13):3573-87.e29.
102. Korsunsky I, Millard N, Fan J, Slowikowski K, Zhang F, Wei K, et al. Fast, sensitive and accurate integration of single-cell data with Harmony. *Nature methods.* 2019;16(12):1289-96.
103. Aran D, Looney AP, Liu L, Wu E, Fong V, Hsu A, et al. Reference-based analysis of lung single-cell sequencing reveals a transitional profibrotic macrophage. *Nature immunology.* 2019;20(2):163-72.
104. Heng TS, and Painter MW. The Immunological Genome Project: networks of gene expression in immune cells. *Nature immunology.* 2008;9(10):1091-4.
105. Hu C, Li T, Xu Y, Zhang X, Li F, Bai J, et al. CellMarker 2.0: an updated database of manually curated cell markers in human/mouse and web tools based on scRNA-seq data. *Nucleic acids research.* 2023;51(D1):D870-d6.
106. Miller SA, Policastro RA, Sriramkumar S, Lai T, Huntington TD, Ladaika CA, et al. LSD1 and Aberrant DNA Methylation Mediate Persistence of Enteroendocrine Progenitors That Support BRAF-Mutant Colorectal Cancer. *Cancer research.* 2021;81(14):3791-805.
107. Kuleshov MV, Jones MR, Rouillard AD, Fernandez NF, Duan Q, Wang Z, et al. Enrichr: a comprehensive gene set enrichment analysis web server 2016 update. *Nucleic acids research.* 2016;44(W1):W90-7.

## Figure legends

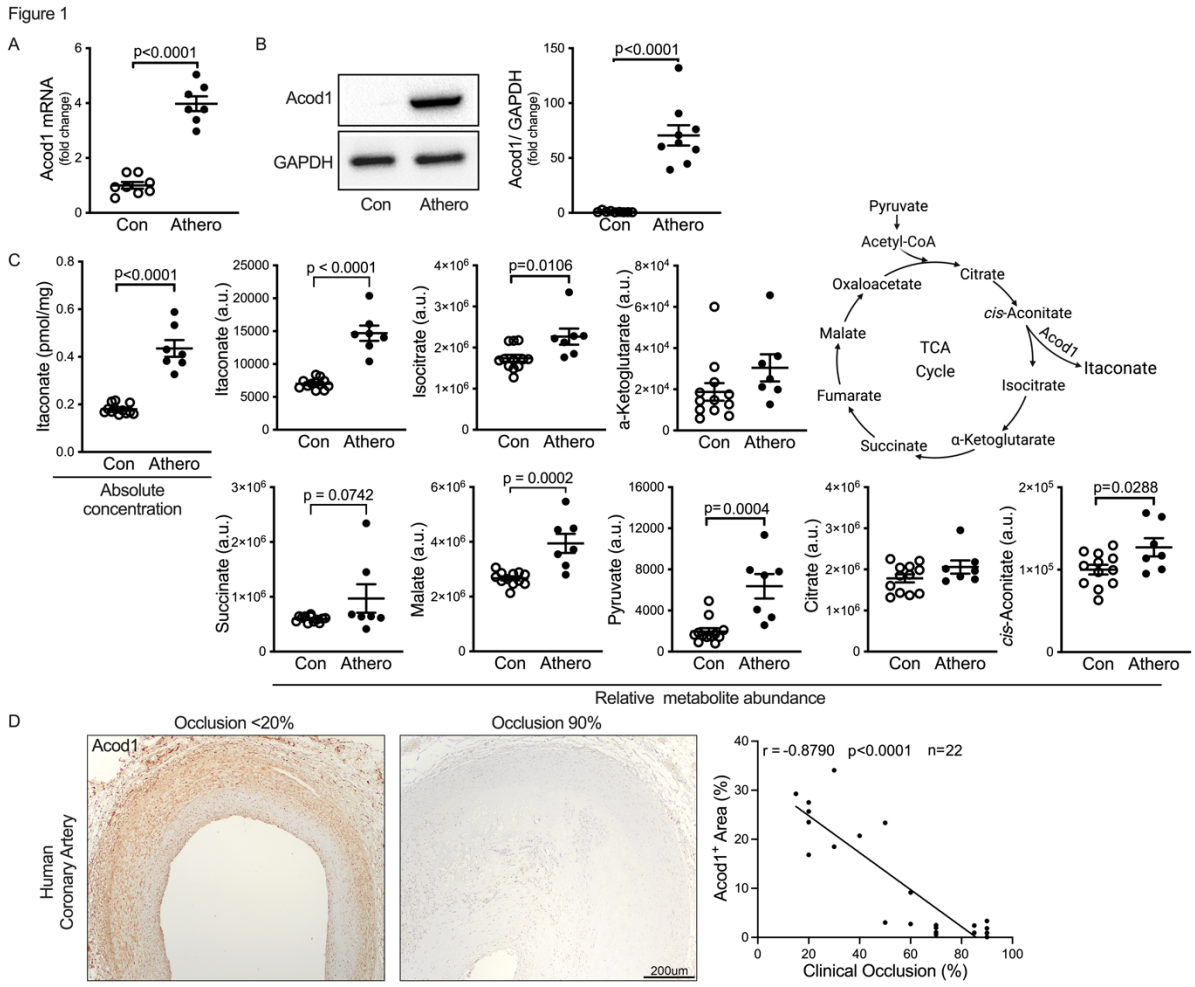


**Figure 1. Acod1 expression and Itaconate production increase in atherosclerotic aorta.** Atherosclerosis was induced by intraperitoneally injecting mice with AAV-PCSK9 and feeding a western-diet (WD) for 10 weeks. **(A)** Acod1 mRNA levels in control (Con, n=8) and atherosclerotic (Athero, n=7) aortas were measured by qRT-PCR. **(B)** Aorta lysates from control (Con) and atherosclerotic (Athero) mice were separated by gel electrophoresis and proteins were detected by western blot with the indicated antibodies. The quantification of Acod1 (n=9/group) after normalization with GAPDH is shown on the right. **(C)** Relative abundance of TCA cycle metabolites (itaconate, isocitrate, α-ketoglutarate, succinate, malate, pyruvate, citrate, *cis*-aconitate) was measured by metabolomics in non-atherosclerotic control (Con, n=12) and atherosclerotic (n=7) aortas. a.u., arbitrary units based on mass spectrometry peak area. The absolute concentrations of itaconate in aortas were also measured. **(D)** Representative images of Acod1-stained human atherosclertic coronary artery. Correlation between the percentage of Acod1 positive area and clinical occlusion using two-sided Pearson correlation analysis is shown on the right (n=22). In **(A-C)**, results are presented as means ± SEM, and unpaired two-tailed Student's t-test was used for statistical analysis.

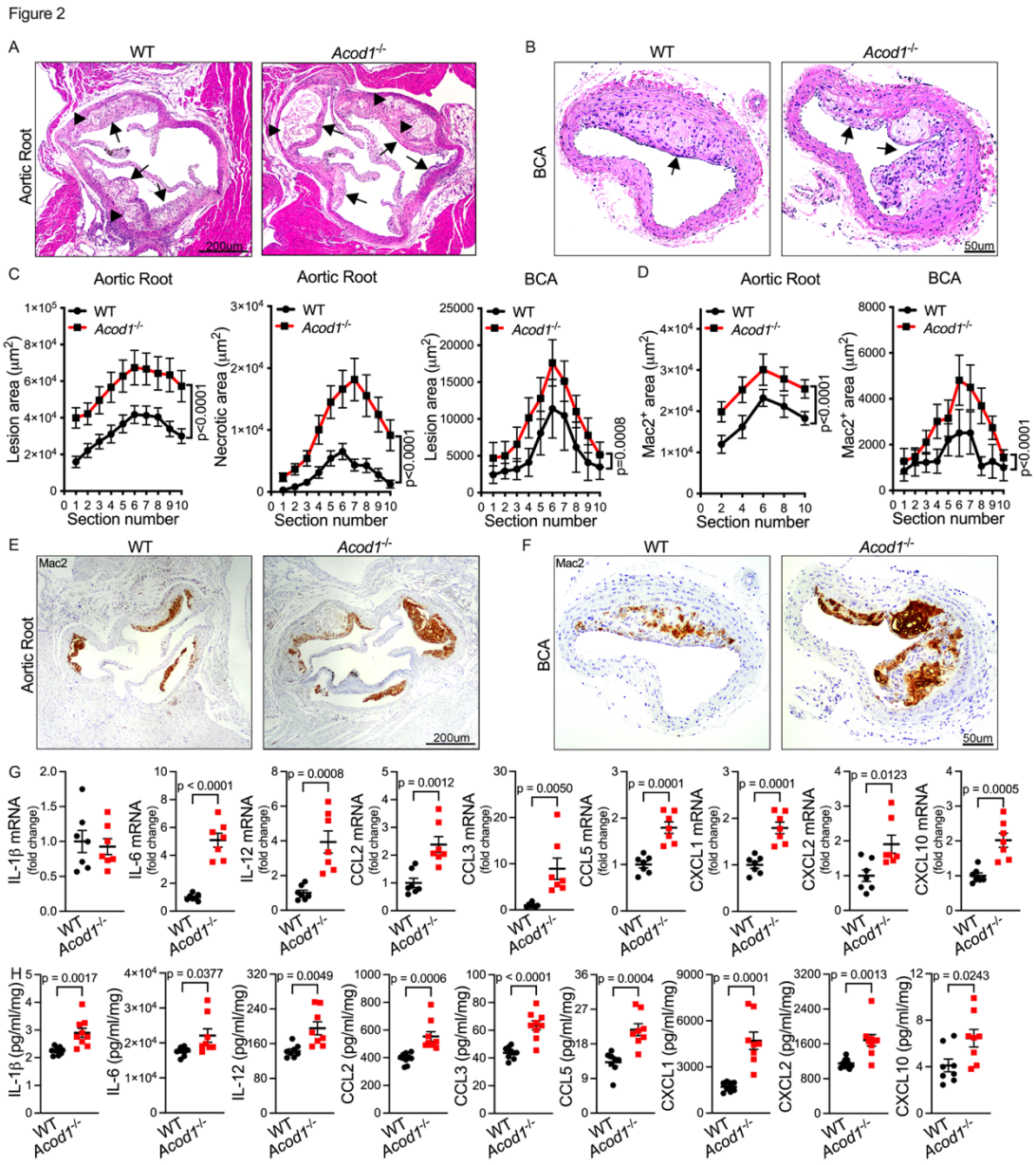


**Figure 2. Acod1 deficiency promotes atherosclerosis by enhancing inflammation.**
WT and *Acod1*$^{-/-}$ mice were induced to become atherosclerotic via PCSK9-AAV administration followed by 10-week western diet. **(A-B)** Representative images of H&E stained **(A)** aortic root and **(B)** brachiocephalic artery (BCA) sections of WT and *Acod1*$^{-/-}$ mice. Arrows indicate atherosclerotic lesions and arrowheads indicate necrotic cores. **(C)** The quantifications of lesion area and necrotic area in each section of aortic root (n=23-24/group) and BCA (n=10/group) are shown. **(D-F)** The quantification of Mac2 positive area in each section of aortic root (n=13/group) and BCA (n=10/group) of atherosclerotic WT and *Acod1*$^{-/-}$ mice is shown **(D)**, with representative images of Mac2-stained **(E)** aortic root and **(F)** BCA sections. **(G-H)** The inflammatory cytokines and chemokines' **(G)** gene expression in atherosclerotic aorta and **(H)** protein levels in tissue culture medium of atherosclerotic aortas from WT and *Acod1*$^{-/-}$ mice, including IL-1β, IL-6, IL-12, CCL2, CCL3, CCL5, CXCL1, CXCL2 and CXCL10 were measured by qRT-PCR (n=7/group) and multiplex assay (n=8-9/group), respectively. Results are presented as means ± SEM. 2-way ANOVA was used in **(C-D)** and unpaired two-tailed Student's t-test was used in **(G-H)** for statistical analysis.

Figure 3

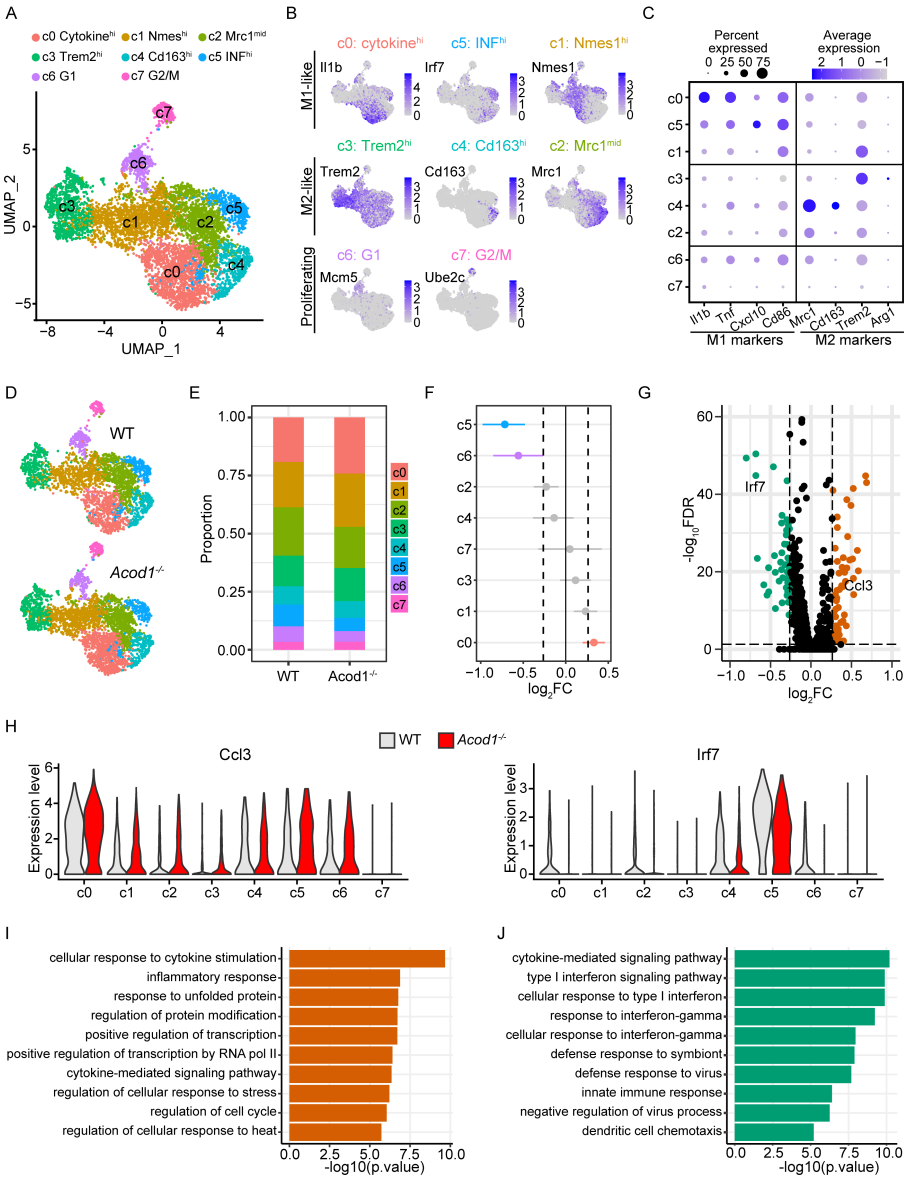


**Figure 3. Single cell analysis of macrophages within the atherosclerotic aorta of WT and *Acod1*$^{-/-}$ mice.** WT and *Acod1*$^{-/-}$ mice were induced to become atherosclerotic via PCSK9-AAV administration followed by 10-week western diet. **(A)** Uniform Manifold Approximation and Projection (UMAP) plot showing eight different macrophage subpopulations revealed by single cell RNA sequencing. **(B)** The expression of representative signature genes from each macrophage subpopulation was overlaid on the UMAP plot. Color intensity indicates normalized expression levels as shown for each gene. **(C)** The expression of M1-like and M2-like marker genes in each macrophage subpopulation was shown. The size of the dots indicates the percentage of cells expressing the gene of interest, while the intensity of the color indicates expression levels. **(D)** UMAP plots of macrophages from atherosclerotic WT and *Acod1*$^{-/-}$ aortas. Clusters were colored as in **(A)**. **(E)** The proportion of macrophage subpopulations from atherosclerotic WT and *Acod1*$^{-/-}$ aortas. **(F)** Differential abundance testing of changes in the proportion of macrophage subpopulations in atherosclerotic *Acod1*$^{-/-}$ aortas. Clusters that passed the threshold of adjusted p values < 0.05 and FC > 1.2 were deemed significant and colored. FC, fold change. **(G)** Volcano plot showing differentially expressed genes in macrophages from atherosclerotic *Acod1*$^{-/-}$ aortas. Up- and down-regulated genes were colored orange and green, respectively. FDR, false discovery rate. **(H)** Violin plots showing the expression of two representative genes, Ccl3 and Irf7, that were differentially expressed between WT and *Acod1*$^{-/-}$ across all macrophage subpopulations. **(I-J)** Gene ontology analysis of **(I)** up- and **(J)** down-regulated genes in macrophages from atherosclerotic *Acod1*$^{-/-}$ aortas.

Figure 4

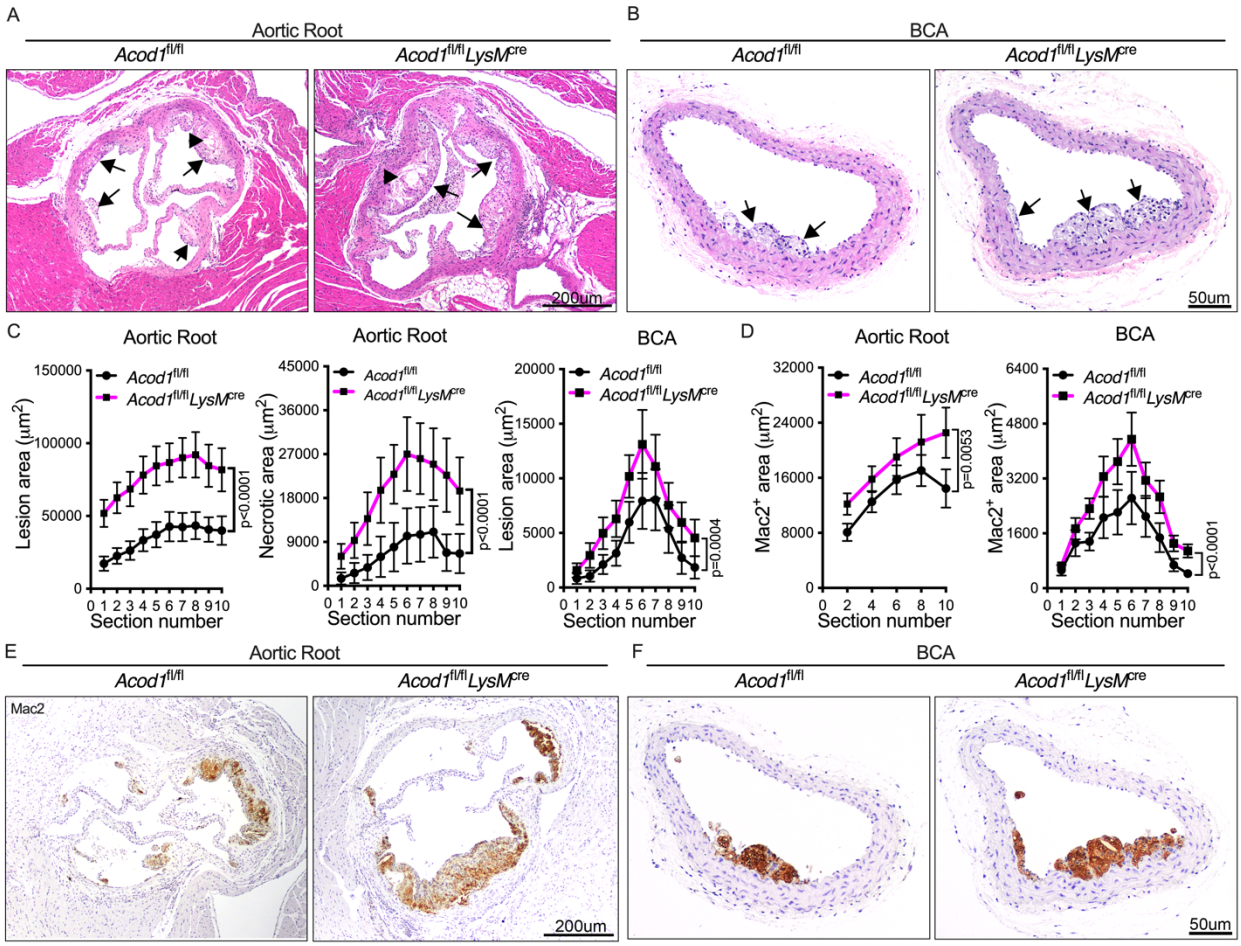


**Figure 4. Acod1 deficiency in myeloid cells confers increased atherogenesis and macrophage infiltration.** *Acod1*$^{fl/fl}$ and *Acod1*$^{fl/fl}$*LysM*$^{cre}$ mice were induced to become atherosclerotic via PCSK9-AAV administration followed by 10-week western diet. **(A-B)** Representative images of H&E stained **(A)** aortic root and **(B)** brachiocephalic artery (BCA) sections of atherosclerotic *Acod1*$^{fl/fl}$ and *Acod1*$^{fl/fl}$*LysM*$^{cre}$ mice. Arrows indicate atherosclerotic lesions and arrowheads indicate necrotic cores. **(C)** The quantifications of lesion area and necrotic area in each section of aortic root (n=17-20/group) and BCA (n=17-19/group) are shown. **(D-F)** The quantification of Mac2 positive area in each section of aortic root (n=9/group) and BCA (n=11-13/group) of atherosclerotic *Acod1*$^{fl/fl}$ and *Acod1*$^{fl/fl}$*LysM*$^{cre}$ mice is shown **(D)**, along with representative images of Mac2-stained **(E)** aortic root and **(F)** BCA sections. Results are shown as means ± SEM. 2-way ANOVA was used for statistical analysis. P values indicate the main effect of the comparison.

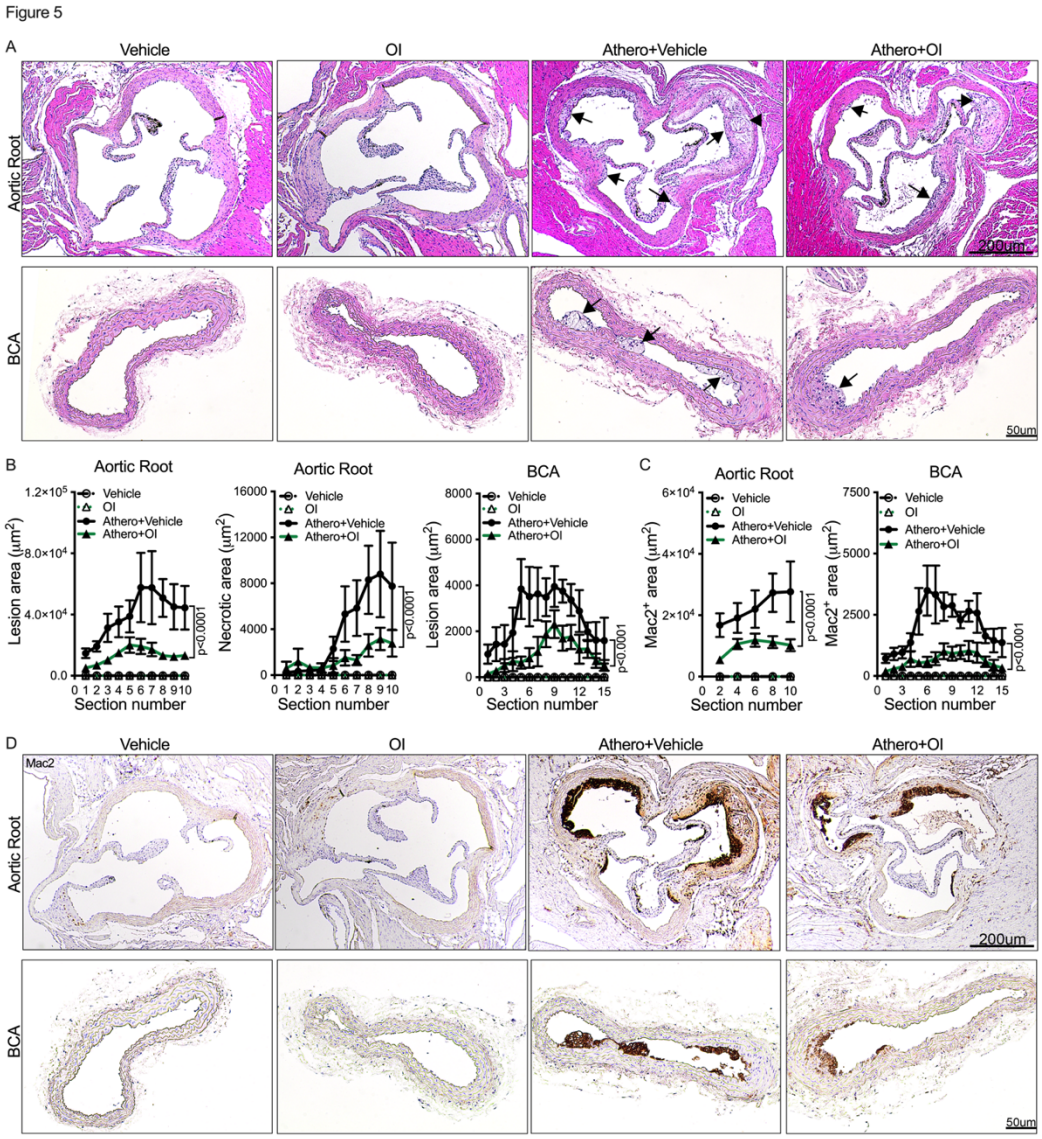


**Figure 5. Itaconate derivative 4-octyl itaconate inhibits atherogenesis.**
**(A)** Representative images of H&E-stained aortic root and brachiocephalic artery (BCA) sections of mice with indicated treatment. Vehicle: vehicle control; OI: 4-octyl itaconate; Athero+Vehicle: atherosclerosis and vehicle; Athero+OI: atherosclerosis and 4-octyl itaconate. Arrows indicate atherosclerotic lesions and arrowheads indicate necrotic cores. **(B-C)** The quantifications of lesion area and necrotic area **(B)** as well as Mac2 positive area **(C)** in each section of aortic root and BCA from indicated mice are shown (n=7-8/group). **(D)** Representative images of Mac2-stained aortic root and BCA sections of mice with indicated treatment. Results are shown as means ± SEM. 2-way ANOVA followed by Tukey's post hoc test was used for statistical analysis. P values indicate the main effect of the comparison between Athero+Vehicle vs. Athero+OI.

Figure 6

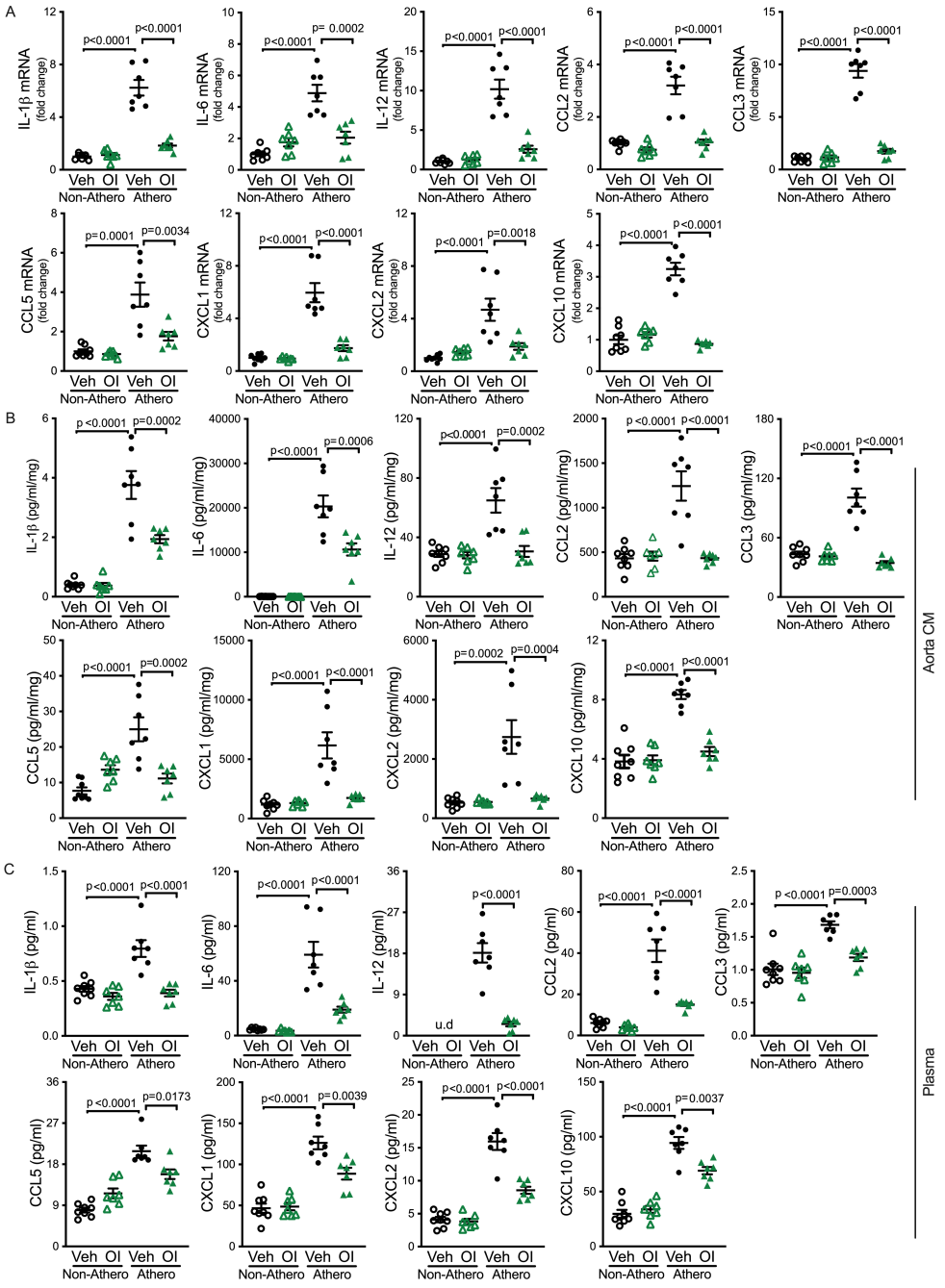


**Figure 6. 4-octyl itaconate attenuates inflammation caused by atherosclerosis.**
WT mice were subjected to the following treatments: 4-octyl itaconate (OI) only, atherosclerosis (Athero) only and OI plus Athero. Vehicle was used as the control for OI, and mice without atherosclerosis (Non-Athero) were used as control mice. **(A)** Gene expression of inflammatory cytokines and chemokines including IL-1β, IL-6, IL-12, CCL2, CCL3, CCL5, CXCL1, CXCL2 and CXCL10 in aorta of indicated mice were measured by qRT-PCR (n=7-8/group). **(B-C)** The protein levels of inflammatory cytokines and chemokines including IL-1β, IL-6, IL-12, CCL2, CCL3, CCL5, CXCL1, CXCL2 and CXCL10 in **(B)** tissue culture medium (CM) of aortas or **(C)** plasma of indicated mice were determined by multiplex assay (n=7-8/group). u.d: undetectable. Protein levels in aorta CM were normalized to tissue weight for analysis. Results are presented as means ± SEM. 2-way ANOVA followed by Tukey's post hoc test was used for statistical analysis.

Figure 7

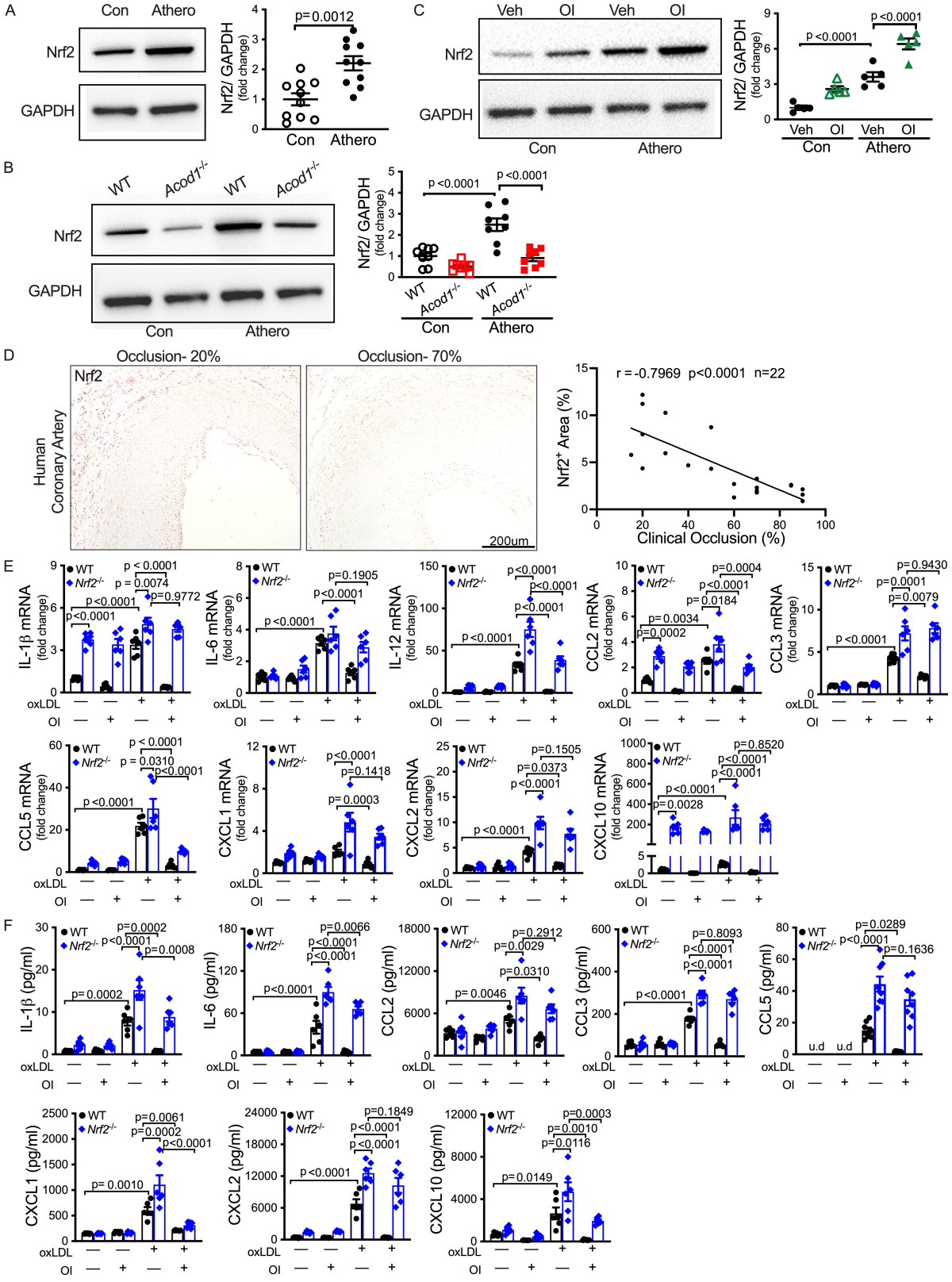
A
Con
Athero
Nrf2
GAPDH
Nrf2/ GAPDH (fold change)
p=0.0012
Con
Athero
B
WT
Acod1-/-
WT
Acod1-/-
Nrf2
GAPDH
Con
Athero
p <0.0001
p <0.0001
Nrf2/ GAPDH (fold change)
C
Veh
OI
Veh
OI
Nrf2
GAPDH
Con
Athero
p <0.0001
p <0.0001
Nrf2/ GAPDH (fold change)
Veh
OI
Veh
OI
Con
Athero
D
Occlusion- 20%
Occlusion- 70%
Nrf2
Human Coronary Artery
200um
r = -0.7969 p<0.0001 n=22
Nrf2+ Area (%)
Clinical Occlusion (%)
E
IL-1β mRNA (fold change)
IL-6 mRNA (fold change)
IL-12 mRNA (fold change)
CCL2 mRNA (fold change)
CCL3 mRNA (fold change)
CCL5 mRNA (fold change)
CXCL1 mRNA (fold change)
CXCL2 mRNA (fold change)
CXCL10 mRNA (fold change)
WT
Nrf2-/-
oxLDL
OI
F
IL-1β (pg/ml)
IL-6 (pg/ml)
CCL2 (pg/ml)
CCL3 (pg/ml)
CCL5 (pg/ml)
u.d
u.d
CXCL1 (pg/ml)
CXCL2 (pg/ml)
CXCL10 (pg/ml)
WT
Nrf2-/-
oxLDL
OI

**Figure 7. Nrf2 signaling is importantly involved in suppressing atherogenesis and inflammation mediated by itaconate. (A)** Whole cell lysates were extracted from aortas of mice with or without atherosclerosis, and the protein level of Nrf2 was determined by western blot. The quantification is shown on the right (n=10/group). **(B)** Aorta lysates from WT and *Acod1*$^{-/-}$ mice with or without atherosclerosis were extracted, and Nrf2 protein level was determined by western blot. The quantifications of Nrf2 (n=8/group) that were normalized with GAPDH are shown on the right. **(C)** Aorta lysates from WT mice (with or without atherosclerosis) that were subjected to 4-octyl itaconate (OI) administration or vehicle control (Veh) were immunoblotted against Nrf2. Quantification is shown on the right (n=5/group). GAPDH was used as loading control in **(A-C)**. Con: control. Athero: atherosclerosis. **(D)** Representative images of Nrf2-stained human atherosclerotic coronary artery. Correlation between the percentage of Nrf2 positive area and clinical occlusion using two-sided Pearson correlation analysis is shown on the right (n=22). **(E-F)** Bone marrow derived macrophages (BMDMs) from WT and *Nrf2*$^{-/-}$ mice were treated with or without OI (250 μM), followed by exposure to oxLDL (100 μg/ml). Vehicle was used as control. Cells and culture medium supernatant were collected at the end of experiment, and RNA was extracted from the cells. The inflammatory cytokines' and chemokines' **(E)** gene expression in those BMDMs and **(F)** protein levels in the culture media, including IL-1β, IL-6, IL-12, CCL2, CCL3, CCL5, CXCL1, CXCL2 and CXCL10 were measured by qRT-PCR and multiplex assay, respectively (n=6/group). u.d: undetectable. Results are presented as means ± SEM. Unpaired two-tailed Student's t-test was used in **(A)** and 2-way ANOVA was used in **(B-C)** and **(E-F)** for statistical analysis.